Bulletin of Geophysics and Oceanography Vol. 66, n. 4, pp. 357-388; December 2025
DOI 10.4430/bgo00512

Geophysical assessment for earthquake mitigation: probabilistic seismic hazard analysis and Earth gravity inversion in the Sorong fault zone, West Papua, Indonesia

R. Lewerissa[1], L.A.S. Lapono[2], R. Tandirerung[3] and R.D. Indriana[4]

[1] *Department of Physics, Papua University, Manokwari, Papua Barat, Indonesia*
[2] *Department of Physics, Nusa Cendana University, Nusa Tenggara Timur, Kupang, Indonesia*
[3] *Department of Geological Engineering, Papua University, Manokwari, Papua Barat, Indonesia*
[4] *Department of Physics, Diponegoro University, Semarang, Jawa Tengah, Indonesia*

(Received: 18 June 2025; accepted: 22 October 2025; published online: 12 December 2025)

ABSTRACT This study integrated seismological and gravity analyses to understand the tectonic characteristics and seismic hazard potential of the Sorong fault zone in Papua, Indonesia. Seismic data map hypocentre distribution, analyse seismicity, and calculate peak ground acceleration (*PGA*) and spectral acceleration (*Sa*) within a probabilistic seismic hazard analysis (PSHA). Bouguer gravity data were analysed through regional-residual anomaly separation, two-dimensional and three-dimensional (3D) Euler deconvolution (ED), and 3D gravity inversion to estimate the subsurface density distribution and fault geometry. The seismicity parameter analysis indicated a magnitude of completeness (M_c) of 4.5 and a *b*-value of 0.93±0.29, reflecting a balance between large and small earthquakes and indicating high stress in the region. The PSHA based on the Sorong fault source in the Dampier segment showed *PGA* values ranging from 0.016 to 0.265 g for a 50-year return period. The *Sa* for periods of 0.2, 0.3, 0.6, 1.0, and 2.0 s shows maximum values for short periods, and vice versa. These results are consistent with the regional and global PSHA analyses for Papua Island. Gravity data analysis showed spectral differences between shallow and deep sources, suggesting a clear differentiation in the rheology of the deep and shallow crust; therefore, the two zones exhibit different mechanical behaviours. The ED identifies clusters of solutions potentially associated with the Sorong fault segments despite the interpretative limitations inherent to the method. The 3D gravity inversion suggests the presence of high-density zones interpreted as magmatic intrusions and low-density zones related to shear zones or deformed rocks, pending further validation of this interpretation. A comparison suggests a possible spatial relationship between the density anomaly zones and the concentrations of seismic activity, which may reflect the structural configuration of active faults. These findings enhance our understanding of tectonic mechanisms and contribute to seismic hazard assessments of the Sorong fault zone.

Key words: earthquake, PSHA, Bird's Head, gravity modelling.

1. Introduction

Eastern Indonesia, including West Papua, has a complex tectonic setting that involves plate interactions, subduction zones, and fault systems. This contributes to the diversity of seismic hazards. West Papua is located in the convergence zone between the Caroline and Indo-Australian plates. The Caroline plate subducts in the New Guinea Trough, with a smaller subduction zone developing in the Manokwari Trough (Hutchings and Mooney, 2021). The complex tectonic structure is characterised by shear fault zones that accommodate E-W trending sinistral movements. Shear faults play an important role in accommodating oblique convergence between tectonic plates. Movement occurs between the Pacific plate (including the Philippine Sea plate and Caroline plate) and the Indo-Australian plate. The Sorong fault, oriented E-W, extends from the Bird's Head peninsula to near East Sulawesi. West of Bird's Head, this fault splits into several 'ponytail' faults (Watkinson and Hall, 2017; Hutchings and Mooney, 2021).

The Sorong fault system is an important tectonic feature in West Papua, with variable seismicity. Seismic activity remained low near Bird's Head, with no strike-slip faults above a magnitude of 5.0. Near Halmahera Island, strike-slip faulting of magnitude larger than, or equal to, 5.0 has increased, with a slip rate of 19 mm/yr. The western branch of the Sorong fault caused significant earthquakes, such as a moment magnitude (M_w) 7.2 earthquake in 2019 in southern Halmahera. This fault is linked to the Yapen fault east of the Bird's Head peninsula, although some studies suggest that sinistral shear may divert south from the Yapen fault to the Tarera-Aiduna fault, bypassing the Sorong fault in Bird's Head (Hutchings and Mooney, 2021). The Sorong fault accommodates complex oblique convergence in eastern Indonesia through interactions with other fault systems and serves as a major tectonic element with implications for regional seismic hazards.

Previous studies related to seismotectonics in the Bird's Head region of Papua have been conducted. A study on fault activity and earthquake risk in eastern Indonesia used a combination of approaches: analysis of tectonic geomorphology and drainage patterns, observation of exposed faults, and historical seismicity. The study concluded that eastern Indonesia faces significant seismic risks, with the potential for large earthquakes, tsunamis, and urban impacts. Tectonic complexity and active faults contribute to the high seismic risk in this region (Watkinson and Hall, 2017). The Sorong fault in West Papua, running from north of Salawati through Sorong city towards Manokwari, features a 15-kilometre-wide zone of linear ridges and valleys trending NE-SW. Despite being considered inactive by many researchers, evidence shows Quaternary activity and major earthquakes in 1937 (M 6.9) and 1944 (M 7.2 and 7.4), with left-lateral shear focal mechanisms. Based on its 420-kilometre length and lack of significant step-over, the Sorong fault could generate $M > 8.0$ earthquakes (Watkinson and Hall, 2017).

Research on ancient granite rocks found in the north-western part of Papua Island has been conducted using field approaches and rock sampling, petrographic and whole-rock geochemical analyses, uranium-lead (U-Pb) zircon geochronology, and cathodoluminescence imaging (Jost *et al*., 2018). Two main episodes of magmatism were identified in West Papua: a) a Palaeozoic episode: Late Devonian to Late Mississippian (363-324 million years ago), and b) a Mesozoic episode: Late Permian to Late Triassic (257-223 million years ago). Both episodes occurred in continental margin environments above subduction zones, with Permian-Triassic granitoids showing clear evidence, whereas Devonian-Carbon granitoids are interpreted as post-orogenic magmatism. This study reveals complex intrusive bodies in West Papua that are partly obscured by left-slip faults along the Sorong fault system, with some granitoid bodies being displaced by the fault system.

A kinematic model analysis of the 5,000-kilometre Indonesia-Australia-Papua New Guinea collision zone was conducted using 267 Global Positioning System (GPS) velocities and 492 earthquake slip vectors (Zhao *et al*., 2023). This model provides an integrated understanding of tectonic interactions in this region. This study proposes a new model for West Papua by dividing it into eight micro-blocks, improving on previous studies that considered West Papua as a single block. The model provides precise quantification of slip rates along major faults, such as the Yapen and Tarera-Aiduna faults. These estimates are consistent with previous seismic studies but offer greater accuracy, although they are limited by the reliance on a few GPS observations (267 velocities) over a very large area. This sparse data coverage can lead to uncertainties in the model, particularly in areas with limited observations. Although previous research has provided valuable insights into the seismotectonic characteristics of the Bird's Head region in Papua, a significant gap remains in our understanding of the seismic hazards. A comprehensive seismic hazard assessment is crucial for effective earthquake risk mitigation in tectonically active regions.

Our research utilises an analytical framework that integrates the seismicity parameter magnitude of completeness (M_c), along with the *a* and *b* values, as key variables in probabilistic seismic hazard analysis (PSHA). Furthermore, we applied the gravity method by modelling the inversion of Earth's gravity anomaly to assess seismic hazards in the Bird's Head region of Papua, with particular emphasis on the Sorong fault zone. PSHA is a methodological approach for evaluating seismic hazards in a given area. This approach forms the basis for most seismic building code regulations (Sokolov *et al*., 2024) This method integrates earthquake source characteristics, path effects, and local site response while accounting for uncertainties in the calculations (Gerstenberger *et al*., 2020; Badreldin *et al*., 2024). PSHA estimates ground motion parameters, such as peak ground acceleration (*PGA*) and spectral acceleration (*Sa*), for various exceedance probabilities over a specified time period. The M_c parameter, the lowest magnitude above which all events can be fully detected, is a critical parameter for seismicity studies and the determination of the *b*-value, which is a critical parameter for the probability of seismic hazard assessment and is strictly related to faulting mechanisms (Ali and Akkoyunlu, 2022).

The gravity method is a geophysical technique used to map and explore subsurface structures on the Earth. Gravity field data are crucial for structural mapping, particularly for acquiring information on geological formations. These data display signals with a broad dynamic amplitude range influenced by the geometries, depths, and density characteristics of the sources (Eldosouky and Saada, 2020; Thanh Pham *et al*., 2021). The gravity method provides high-resolution structural interpretations with enhanced lateral resolution compared with other geophysical techniques. It is particularly effective for analysing lateral variations in lithospheric density, fluctuations in density interfaces, and deep structural features (Li *et al*., 2025). In this study, gravity anomaly inversion modelling was employed to precisely identify subsurface geological structures, particularly the Sorong fault and its segments, as well as lithospheric boundaries that may influence seismic activity in the study area. Faults, which are discontinuities in the Earth's crust caused by stress, are generally classified into normal, reverse, and strike-slip faults based on their geometry and displacement. In this context, gravity data can provide significant constraints on the geometry of subsurface faults and lithospheric structures, thereby improving the accuracy of the source models used in PSHA.

The displacement length of faults can range from a few centimetres to hundreds of kilometres, making it crucial to recognise their characteristics, density, and geometric distribution (Essa *et al*., 2021). The integration of these two methods is expected to provide a more holistic approach for detailed seismic hazard assessment, especially in regions with high tectonic complexity, such

as the western part of Papua Island, and to serve as a foundation for more effective disaster mitigation planning in areas vulnerable to earthquakes.

2. Tectonic and geological setting of Sorong

From the Miocene to the Pliocene, the Australian plate boundary experienced two encounters between the island and continental arcs when the Eocene-Miocene island arc fragments collided with northern Papua. Intermediate felsic igneous activity occurred during the Middle Miocene. This activity was related to oblique subduction beneath New Guinea (Papua) before the collision between the island arc and continent or partial melting associated with crustal thickening during the Miocene collision. After the middle Miocene rock formation, another phase of magmatism occurred during the Plio-Pleistocene. This recent phase has been recorded in central and eastern New Guinea (Papua) and has produced valuable mineral concentrations, including one of the world's largest copper and gold deposits. These rocks result from magma fluids originating in the Earth's mantle and are influenced by the continental crust as they form within the thickened crust. Locally, this activity is associated with significant normal faulting that crosses the central highlands of Papua (White *et al*., 2014).

The Sorong fault zone is located on the Bird's Head peninsula in West Papua, New Guinea. It is a major horizontal fault system that shapes the regional geology of NW New Guinea. The Sorong fault zone exhibits left-lateral movement, where blocks on one side move to the left relative to those on the other. After the late island arc-continent collision in the early Pliocene, the Sorong and Ransiki fault zones facilitated the 300-kilometre westward movement of the Tamrau, Tosem, and Arfak blocks (Webb *et al*., 2020). Major movements along the Sorong fault zone occurred during the Plio-Pleistocene period, following an early Pliocene collision. The displacement along the Sorong fault zone matches a plate movement of 10 cm/yr for the Pacific-Caroline plate over the last three million years.

The Sorong fault system is a significant geological feature in north-western Papua and plays an important role in the tectonic setting and intrusive body arrangement of the region. The Sorong fault system is one of the two visible left-lateral strike-slip fault zones on the Bird's Head peninsula, the other being the Ransiki fault system. This system crosses the northern peninsula of the country. The fault system juxtaposes younger Eocene-Miocene volcanic arc fragments in the north and NW with older Gondwanan (Australian) material in the south and SW. The Sorong fault system affects the arrangement of intrusive bodies, leading to the displacement and truncation of granitoid bodies. The Netoni intrusive complex is bounded by the Sorong fault system. The Sorong Granite lies west of the Netoni intrusive complex and is bounded by the Sorong fault system (Jost *et al*., 2018).

Similarities between the Netoni intrusive complex, Wariki Granodiorite, and Anggi intrusive complex indicate displacements of at least 30 km along the Sorong fault system. The Sorong fault system has caused strong cataclastic deformation in outcrops, particularly in the Sorong Granite. These observations highlight the role of the Sorong fault system in shaping the geological configuration of north-western Papua, specifically in granitoid body distribution and deformation (Fig. 1). This study adds information on the main Sorong fault in the Bird's Head of Papua, which is a crucial seismic source in the region. The fault source shares geometric attributes with diffuse seismicity sources while simplifying the aspects of the source definition (Table 1). The Sorong fault is a strike-slip fault extending hundreds of kilometres, connecting the subduction margin east of the continental collision zone to the west. The Sorong fault is part of the collision zone

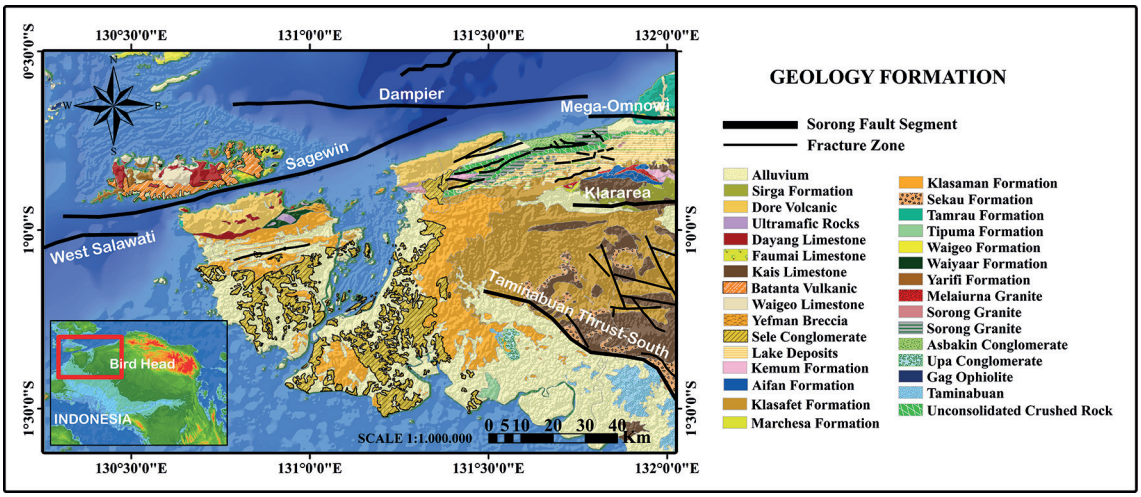

Fig. 1 - Geologic map of the Sorong fault zone in the Bird's Head peninsula of Papua [based on Amri and Harahap (1990)].

Table 1 - Data and source parameters of the Sorong and Taminabuan faults in the Bird's Head of Papua Island (PuSGeN, 2017).

No.	Structure		Slip-rate (Mm/yr)	Sense Mechanism	Dip	Top	Bottom	L (km)	M_{max}
	Main	Segment							
1.	Sorong fault	Sagewin	12.5	Strike-slip sinistral	90	3	18	125	7.2
2.	Sorong fault	Dampier	5.0	Strike-slip sinistral	90	3	18	111	7.1
3.	Sorong fault	Mega-Omnowi	5.0	Strike-slip sinistral	90	3	18	193	7.7
4.	Sorong fault	Klararea	1.5	Strike-slip sinistral	90	3	18	90	7.3
5.	Taminabuan Thurst	South	0.1	Thurst	45NE	3	18	242	6.5

between the Australian and Pacific plates.

The Sorong fault segments have a sinistral strike-slip mechanism that involves movement within the Earth's crust. This mechanism involves horizontal movement, where two blocks of rock slide laterally. Movement occurs along the fault with a shear component to the left (sinistral) when viewed from the observer's direction and usually occurs on transform or horizontal faults. The Taminabuan thrust (TT) is a key fault in Bird's Head, a N-NE-trending fold that is important for regional rock uplift and deformation. This fault was formed because of pressure and deformation during the continental collision. Through subduction and uplift, the TT contributes to mountain and rock folding formations in Bird's Head of Papua. This activity uplifts older rocks to the surface, and forms distinct mountain ranges. Rock deformation produces folds, fractures, and faults that are visible in the surface rocks.

3. Research methods

This study was divided into two main stages. The first stage involved evaluating earthquake hazards based on the multi-site PSHA approach for key locations in the Bird's Head region of

Papua, including the Sorong fault system line, includes the city and regency of Sorong in the south-western Papua province. The second stage involved modelling the Earth's gravity data to obtain the subsurface structure in the study area. To evaluate earthquake hazards at a location, it is necessary to divide seismically homogeneous geological subregions, which are defined as seismic sources (Gregori and Christiansen, 2018). Within a zone, the source is uniform and homogeneous; therefore, every point within the source has the same potential to produce an earthquake (Rahman and Bai, 2018). This research area follows earthquake event distribution in the Bird's Head region of Papua Island, specifically in the Sorong region and its surroundings as the main Sorong strike-slip fault line at coordinates 129° - 133° E and 0.5° N - 3° S.

3.1. Research data collection

3.1.1. Earthquake data for the Bird's Head region of Papua on the Sorong fault zone

The earthquake data used were historical earthquakes from the Bird's Head region of Papua Island, particularly the Sorong fault line in the south-western Papua province (Fig. 2). The data were sourced from the United States Geological Survey (USGS) and the International Seismological Centre (ISC) based on extraction from the Incorporated Research Institutions for Seismology Data Management Center (IRIS DMC) using ZMAP 7 software (Reyes and Wiemer, 2019). Earthquake data were collected for the 1963-2024 period, with magnitudes from 3.5 to 7.4 M_w at depths of 0–458.1 km (Fig. 2a). More than 2,782 earthquakes have occurred on the Sorong fault line in Bird's Head of Papua, dominated by shallow earthquakes (Fig. 2b). The selection of the earthquake catalogue period was guided by technical considerations, including global seismic data quality, consistency, availability of recording instruments, and the distribution of monitoring stations. Earthquake catalogues help understand the distribution of earthquakes in space and time and the proportion of large and small earthquakes. Based on the earthquake catalogue of the Bird's Head region of Papua on the Sorong fault, magnitude homogenisation was performed using the same scale (Fig. 3). Magnitude homogenisation uses regression analysis between pairs of magnitude scales to convert the magnitude into a single M_w scale.

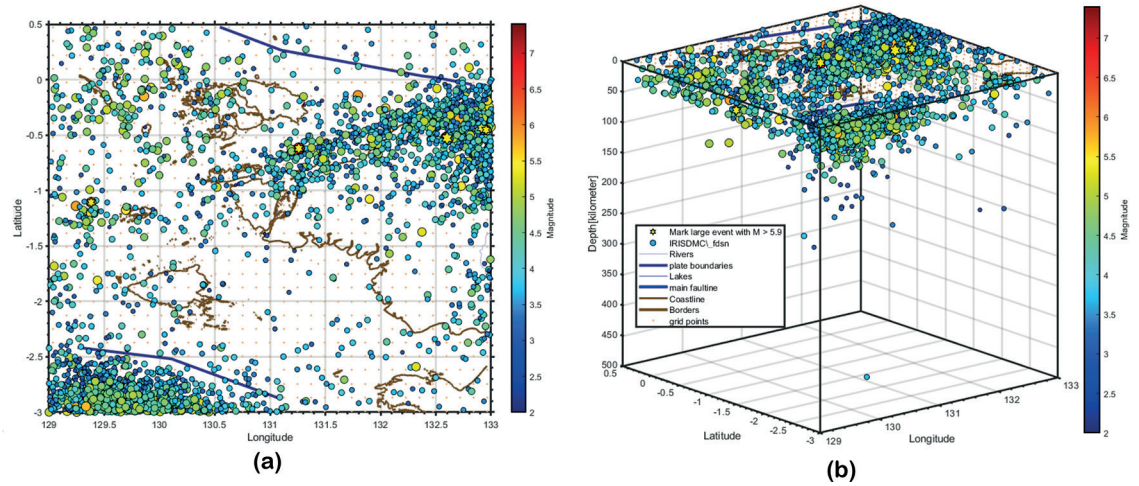

Fig. 2 - Distribution of earthquakes in the Bird's Head region of Papua on the Sorong fault line in the south-western Papua province for the 1964-2024 time period (a); 3D model of earthquake distribution in the Sorong fault line region, which shows that it is dominated by shallow earthquakes (b).

The globally recognised empirical relationship equation for converting the magnitude expressed in M_b to M_W is (Scordilis, 2006; Di Giacomo *et al*., 2015; Lewerissa *et al*., 2021):

$$M_W = 0.85\, M_b + 1.03; 3.5 \leq M_b \leq 6.2\,. \quad (1)$$

To convert M_L to M_W, a globally recognised equation is used to a large extent (Malagnini and Munafò, 2018; Lewerissa *et al*., 2021):

$$M_W = \frac{2}{3}\, M_L + 1.14;\ M_L \leq 4.3\,. \quad (2)$$

A declustering process was applied to the Bird's Head Papua earthquake catalogue on the Sorong fault line to separate foreshocks and aftershocks from the main earthquakes using the Reasenberg (1985) algorithm with ZMAP 7 software (Reyes and Wiemer, 2019). The Reasenberg method determines aftershocks by clustering earthquakes according to their temporal and spatial interaction zones using Omori´s law and stress distribution (Benali *et al*., 2023).

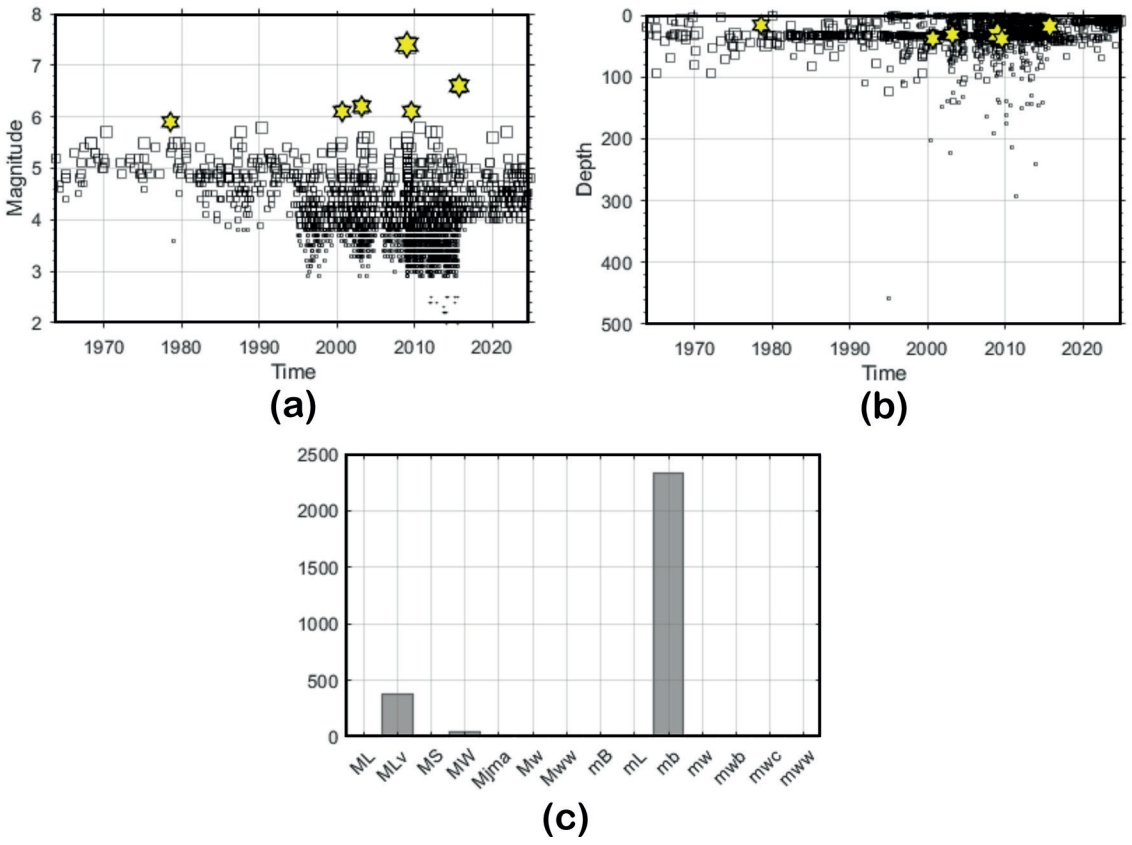

Fig. 3 - Distribution of earthquake magnitude over time (a), distribution of earthquake depth over time (b), and type of earthquake magnitude used for magnitude homogenisation (c).

3.1.2. World Gravity Map of 2012

Gravity anomaly data for the Bird's Head region of Papua on the Sorong fault line in West Papua were modelled using the World Gravity Map of 2012 (WGM2012) (https://bgi.obs-mip.fr/). The WGM is a high-resolution gravity data compilation produced by the Bureau Gravimétrique International and several international organisations, including the Commission on Geological Maps of the World, UNESCO, the International Association of Geodesy, the International Union of Geodesy and Geophysics, and the International Union of Geological Sciences. The model combines satellite gravity data with global land and ocean gravity data in spherical geometry. The gravity anomalies in the WGM2012 were derived from the Earth Gravitational Model 2008 and geopotential model (Balmino *et al*., 2012; Lewerissa *et al*., 2023; Ali *et al*., 2024).

The WGM2012 is available at a two-arcmin resolution (approximately 3.66 km) and provides gravity-related products, including free-air (FA) anomalies, complete spherical Bouguer anomalies, gravitational perturbations, and isostasy. WGM2012 provides homogeneous information about the Earth's static gravity field on global and regional scales, making it suitable for geophysical applications (De Lima *et al*., 2023).

The gravity anomaly data included the FA and complete Bouguer anomalies. The complete Bouguer anomaly in the Sorong region ranges from 160.15 mGal to 316.40 mGal (Fig. 4a), while the FA anomaly ranges from -55.47 mGal to 183.37 mGal (Fig. 4b). Furthermore, we incorporated a bathymetry and topography model of the study area derived from the General Bathymetric Chart of the Oceans 2024 (GEBCO_2024), which spans from -2536 to 1033 m (Fig. 5). The study area is predominantly oceanic and reveals traces of several segments of the Sorong fault on the seafloor, including the Sagewin and Dampier faults. Fig. 5 illustrates the linear configuration of the Sorong fault zone, extending from west to east, where the terrestrial topography exhibits a depression aligned with the fault linearity. Compressive or extensional bathymetric-topographic contour patterns indicate the prevailing deformation mechanisms. This bathymetry and topography model served as an input for three-dimensional (3D) gravity anomaly data modelling in the study area.

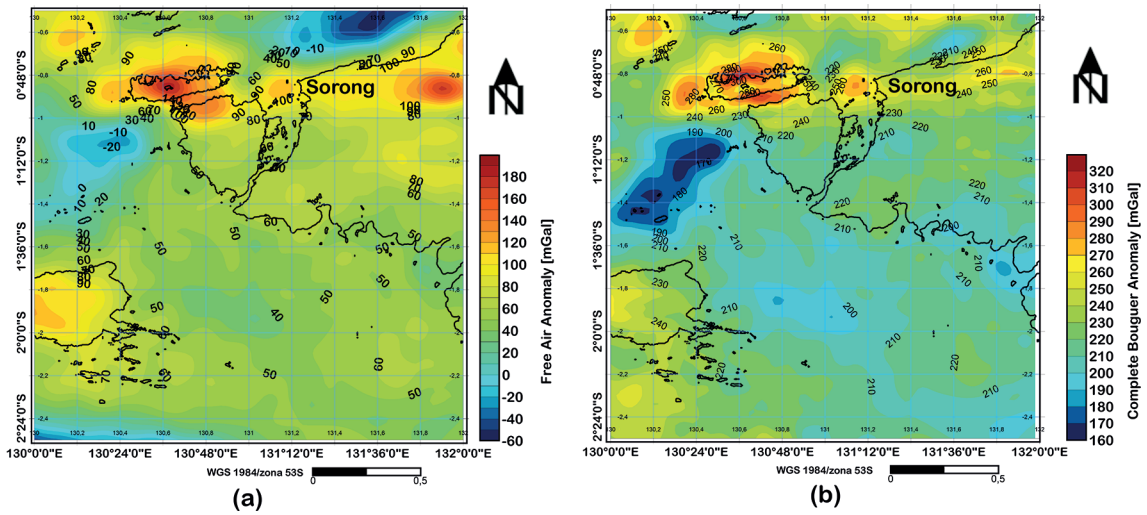

Fig. 4 - Earth's gravity field data attributes based on the WGM2012 model in the Bird's Head of Papua on the Sorong fault zone: a) complete Bouguer anomaly and b) free-air anomaly.

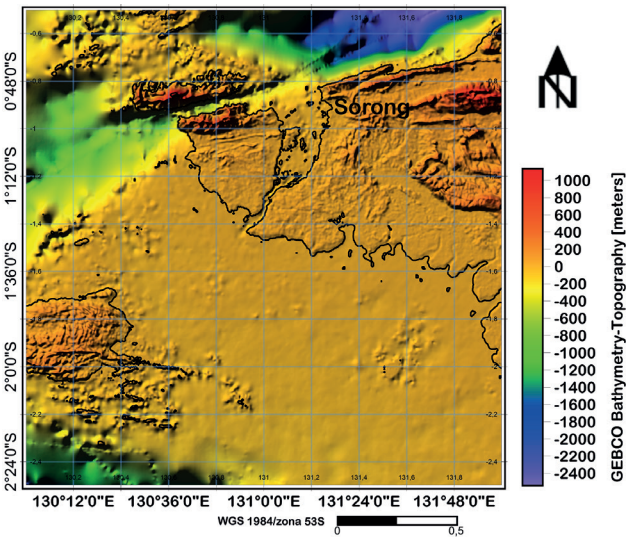

Fig. 5 - The bathymetric and topographic map of the Sorong fault zone, based on the General Bathymetric Chart of the Oceans 2024 (GEBCO_2024) model, shows the dominance of the sea as the main corridor of the Sorong fault segment.

3.2. Estimation of magnitude of completeness (M_c) and seismicity parameters

The observed connection between how often earthquakes occur and their size in a specific area over a given period can be represented as:

$$log_{10} N(M) = a - bM \tag{3}$$

where $N(M)$ is the cumulative number of earthquakes with magnitude greater than, or equal to, magnitude M; a and b are positive. The a parameter is known as seismic activity and depends on many factors, its value ranging from 2 to 8, while the b parameter is known as b-value, generally describing the slope of the trend line of cumulative number and magnitude. A high b-value indicates a larger number of small earthquakes than large earthquakes, whereas a low b-value indicates a smaller number of small earthquakes. b-values are mainly used to measure seismicity and indicate a relative number or ratio, generally ranging from 0.5 to 1.5 (Bora *et al*., 2018).

To calculate seismicity parameters a and b, magnitude completeness (M_c) was first calculated from the Bird's Head Papua earthquake catalogue on the homogeneous Sorong fault line. M_c is an important parameter representing the minimum magnitude recordable by seismic instruments in a region. This parameter is vital for determining earthquake hazard and designing earthquake-resistant structures (Azizi and Saffari, 2024). The maximum curvature method of Wiemer and Wyss (2000) determined M_c using the Gutenberg-Richter equation. Frequency-magnitude plots were constructed for earthquakes in the study area between 1963 and 2024. The maximum curvature point indicates the M_c value, the slope of the red line represents the b-value, and the intercept shows the a-value of the Gutenberg-Richter relationship (Azizi and Saffari, 2024). The calculation of M_c and seismicity parameters (a and b values) for the Sorong fault zone in Sorong city and district was performed using ZMAP 7 software (Reyes and Wiemer, 2019).

We performed spatial and temporal analyses of the b-value to estimate variations in rock properties and stress levels along the Sorong fault line. Spatial and temporal variations in b-values are influenced by stress-dependent characteristics and inversely related to differential stress. A decrease in b-values was observed in hypocentre areas before major earthquakes occurred

(Chiba, 2024). Small *b*-values indicate rock properties such as high stress, fractured media, high deformation rates, or large faults. Small *b*-values are also the opposite of high stress levels and can be used to predict future large earthquakes (Hussain *et al*., 2020).

3.3. Probabilistic seismic hazard analysis

The *PGA* for the Sorong fault zone and its surrounding areas was calculated using seismicity parameters and the multisite PSHA (MPSHA) method. This process utilises REASSESS 2.1 software, which operates on a MATLAB-based Graphical User Interface (GUI) (Chioccarelli *et al*., 2019). The process began with observation points around the Sorong fault zone in the Dampier segment. These points were spaced at 0.2-degree intervals, creating 42 potential sites for the seismic hazard evaluation (Fig. 6a). Seismic source characterisation is vital for assessing seismic hazards. This stage relies on the understanding of the geometry and features of the seismic sources that affect a region (Damanik *et al*., 2023). Seismic source characterisation encompasses various source types to depict earthquake occurrences in different tectonic settings. In this study, we used the Sorong strike-slip fault segment, which influences the city of Sorong and its surrounding areas within a radius of ±200 km, as the main seismic source. The fault source was used to model earthquakes that occurred on shallow crustal faults and on large earthquakes at the subduction interface. Geometrically, the fault source was modelled as a finite plane. This type of source consists of discrete faults with specific movement directions. During the PSHA calculations, ruptures were generated according to the individual earthquake events that might occur on the fault surface (Johnson *et al*., 2021).

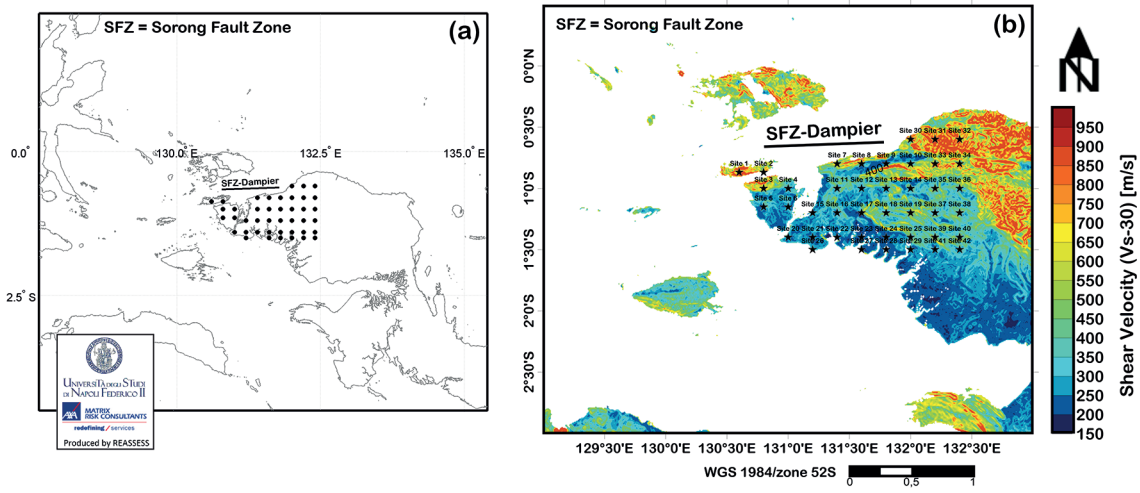

Fig. 6 - PSHA input parameters around the Dampier segment in the Sorong fault zone: a) 42 sites reviewed for seismic hazard assessment and b) shear wave velocity model at a depth of 30 m (V_s-30).

We conducted testing on the Dampier fault segment spanning 111 km, where a major earthquake with an M_w of 6.6 occurred at coordinates –0.620° S and 131.230° E, at a shallow depth of approximately 18.9 km (https://ds.iris.edu/spud/momenttensor/11246225). The Sorong fault on the Dampier segment has a length of 145 km, slip rate of 5 mm/yr, and dip angle of 90°, and features a left-lateral strike-slip mechanism (Table 1). We applied ground motion

prediction equations (GMPE) for three tectonic regions in Indonesia, including the active shallow crust, based on global data from Cauzzi *et al*. (2015). The selection of the GMPE in PSHA is a major challenge in developing models in areas with limited strong ground motion data (Ghasemi *et al*., 2020). As an indicator of the soil quality affecting the seismic response, we used the shear-wave velocity parameter (V_s-30) for the Sorong City area and its surroundings as the PSHA input (Fig. 6b). The V_s-30 values in the area around the Sorong fault zone ranged from 206 to 875 m/s, with low-to-moderate velocities dominating the urban areas in the region.

The V_s-30 values were obtained from the USGS based on an analysis of geomorphological data and topographic slopes (Allen and Wald, 2009). The use of V_s-30 in PSHA helps to estimate ground motion based on local conditions in the study area. *PGA* and *Sa* were measured at a 50-year return period to predict the intensity of ground motion at the study site at periods of 0.2, 0.3, 0.6, 1.0, and 2.0 s. We used the V_s-30 soil classification criteria for the GMPE equation from Cauzzi *et al*. (2015): ≥ 800 m/s (rock); ≥ 360 < 800 m/s (stiff); ≥ 180 < 360 m/s (soft); and < 180 m/s (very soft). Based on the established criteria, the study area lies between soft soil and rock, and the reviewed locations are dominated by V_s-30 values ranging from low to moderate.

3.4. Determination of the depth of regional and residual gravity anomalies

The source depth of the residual and regional gravity anomalies in the Bird's Head of Papua on the Sorong fault line was determined using mean radial spectrum analysis of Bouguer anomaly data. Regional anomalies originating from deep structures are characterised by long wavelengths, whereas residual anomalies linked to shallow structures display short wavelengths (Safani *et al*., 2023). Anomaly source depth is estimated by transforming Bouguer anomaly data to the wave number domain using Fourier transform. The Fast Fourier Transform algorithm was applied to obtain the energy spectrum, and the slope of the straight line in the spectrum curve provided information about shallow and deep anomalous sources (Bencharef *et al*., 2022). Shallow structures affect the high wavenumbers of the power spectrum, whereas deep sources affect low wavenumbers. The depth of the gravity anomaly sources was estimated using the slope of the average radial power spectrum, following the classical approach of Spector and Grant (1970). We applied this approach as a guide for the interpretation and preliminary estimation of the depth of gravity anomaly sources in the complex and heterogeneous Sorong strike-slip fault zone, rather than for the definitive validation of subsurface structure depth. The depth of the source or interface can be estimated by dividing the spectrum into linear segments. Each segment represents the average depth of the source, which can be estimated using:

$$h = \frac{-\left(ln\left(\widetilde{E_2}\right) - ln\left(\widetilde{E_1}\right)\right)}{4\pi(k_2 - k_1)} \tag{4}$$

where h denotes source depth, k denotes wave number, and E_1 and E_2 denote gravity field anomaly values. Each slope reflects a specific part of the source; thus, gravity anomalies can be obtained by filtering the gravity data. The boundary wavenumber should be determined from the lines in the spectrum. In this study, we used the GravPack software for MATLAB-based radial mean spectrum analysis. GravPack is a comprehensive gravity data processing package that performs all steps in a single interface window. The software has a simple GUI with a resolution of 800×600 pixels. GravPack spectral analysis calculates and displays the radially averaged power spectrum of gridded data, enabling source depth estimation (Aydın and İşseven, 2021).

3.5. Euler deconvolution

Euler deconvolution (ED) is a technique used to interpret potential field data, particularly gravity and magnetic data. It automatically estimates the source parameters, specifically the location and depth of subsurface structures. In this study, this method was used to extract the position and depth of linear subsurface features, particularly faults and geological contacts, in the study area. ED is based on the Euler homogeneity equation, which relates the potential field (gravity) and its gradient component to the source location, with the degree of homogeneity expressed as a structural index (Bencharef *et al*., 2022). The ED formula is as follows:

$$(x - x_0)\frac{\partial g}{\partial x} + (y - y_0)\frac{\partial g}{\partial y} + (z - z_0)\frac{\partial g}{\partial z} = N(B - G) \quad (5)$$

where x_0, y_0, and z_0 are the gravity source positions, x, y, and z are the observation points, and $\partial g/\partial x$, $\partial g/\partial y$, and $\partial g/\partial z$ are the measured gravity gradients, N is the structural index, B is the regional value, and G is the measured gravity field.

The structural index N quantifies the rate at which the potential field changes with distance for a specific source geometry. In the context of gravity data, N varies from 0 to 2: N = 0 corresponds to faults (small steps), thin embankments, and sills; N = 1 corresponds to cylindrical and pipe geometries; and N = 2 corresponds to spherical geometries (Bencharef *et al*., 2022). N ranges from 0 to 1, indicating fault structures, whereas an index of 2 represents spherical formations. ED was used to determine the tectonic structure of the region (Kenyo *et al*., 2023). In this study, we performed ED testing with values of 0 and 1 and, subsequently, identified the results that best aligned with the tectonic and geological conditions of the study area. ED identifies clusters of solutions potentially associated with the Sorong fault segments despite the interpretative limitations inherent to the method. We used the Gravmag Suite software to perform ED analysis of the gravity field data in this study. The software was designed to process gravity and magnetic data. It offers a GUI and includes tools for field transformations, refinement filters, semi-quantitative methods, and simple shape-forward modelling algorithms. ED is a semiquantitative technique used to estimate source parameters, delivering reasonably accurate results when applied to well-isolated sources with an appropriate structural index, even if the assumed source shape is only an approximation (Castro *et al*., 2018). However, for sources with complex or irregular geometries, the reliability of estimates may significantly decreased.

3.6. Three-dimensional gravity inversion modelling

3D gravity modelling in Sorong and the surrounding areas was performed using the GravMagInv3D software from the GravMagInv package (https://www.gravmaginv.com/en). Forward and inverse modelling were performed using the grid model. The inversion problem was solved by minimising the residual function using a gradient descent. Three approaches were used for the grid model: grid inversion, lateral inversion, and constant value inversion. The inversion parameters included the iterations, depth strength, and rock density values. The GravMagInv tool allows the inclusion of *a priori* data through regularisation. The residual functional is calculated as the square root of the sum of squares between the calculated and observed values at each observation point, and is formulated as follows (Chepigo, 2023):

$$L = \sqrt{\frac{\sum_{i=1}^{n}(calc_i - obs_i)^2}{N}} \rightarrow minimal \quad (6)$$

where $calc_i$ is the calculated value at the *i*-th point, obs_i is the observed value at the *i*-th point, and *N* is the number of points.

A 3D model grid was developed to represent the physical properties of the subsurface. The model domain was determined by the survey area and target depth, whereas the cell size was set by considering the resolution and computational limits. The model boundaries were defined by the minimum and maximum coordinates on the *x*, *y*, and *z* axes with uniform grid spacing. We used a cell size of 100×100×33, with a model grid density of 2.67 g/cm³ applied throughout to solve forward and inverse problems in gravity exploration (Fig. 7). In the gravity inversion process, a regularisation technique was employed to stabilise the solution while managing the smoothness and complexity of the resulting density models. Topographic and bathymetric models of the Sorong fault zone from GEBCO_2024 were incorporated into the 3D model prior to modelling. In our study, seismicity analysis and PSHA are presented before the gravity modelling results, as the seismic hazard assessment is derived directly from the earthquake catalogue data, which are independent of gravity measurements. Furthermore, gravity analysis serves as a complementary constraint on the tectonic framework, providing 3D structural insights to interpret and validate seismicity patterns, as well as the seismic hazard results in the study area. Gravity analysis is not used as a direct input for PSHA.

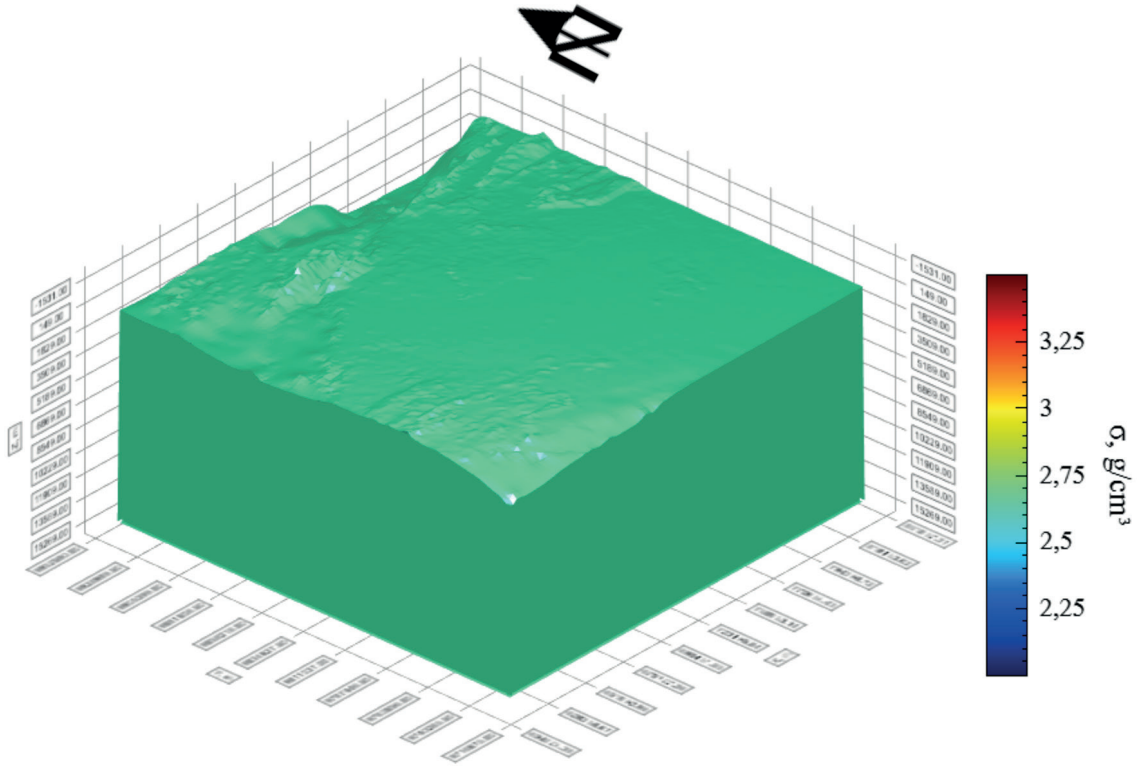

Fig. 7 - The preliminary 3D model for subsurface modelling used the average density of the Earth's crust of 2.67 g/cm³.

4. Results and discussion

4.1. Spatial variation of seismicity parameters of the Bird's Head region in the Sorong fault zone

Following the application of the Reasenberg algorithm for declustering, the number of recorded earthquakes decreased from 2,782 to 333. The spatial distribution of these earthquakes is illustrated in Fig. 8a, which depicts their occurrence along the Sorong fault line within the segments of the south-western Papua province. The 3D distribution of shallow earthquakes is shown in Fig. 8b, which is dominated by earthquakes with a depth less than 50 km. Earthquakes with $M_w > 3.5$ have been recorded continuously since the 2000s (Fig. 8c), whereas earthquake depth variation shows predominantly shallow earthquakes, with five significant events in this area (Fig. 8d).

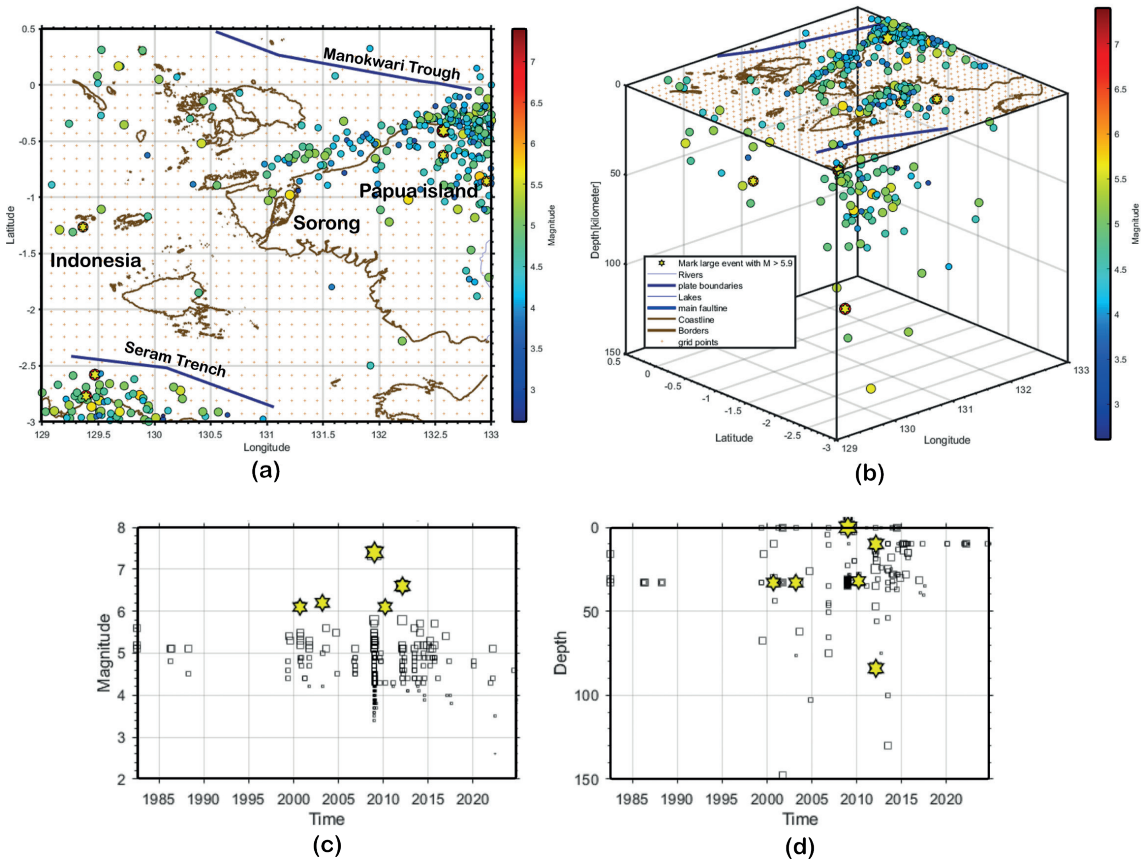

Fig. 8 - Catalogue of earthquakes in the Papua Bird's Head region on the Sorong fault after declustering: a) spatial distribution of earthquakes in *the xy* plane; b) 3D distribution of earthquakes; c) variation in earthquake magnitude over time; and d) variation in earthquake depth over time.

Fig. 8 shows that earthquakes were concentrated on the main strike-slip Sorong fault line in segments including North Kofiau, West Salawati, Sagewin, Dampier, Mega Omnowi, and the Klararea. The observed increase in the number of earthquakes suggests persistent seismic activity, characterised by significant tectonic movements and stress accumulation in Cenderawasih Bay.

Fig. 9 illustrates the frequency and magnitude distribution (FMD) in the Bird's Head region of Papua along the Sorong fault line, as derived from the IRIS DMC earthquake catalogue following homogenisation and Reasenberg declustering for the 1963-2024 period. The maximum likelihood method with bootstrapping yielded an M_c of 4.5. The average seismicity parameter *a* is 6.6, annualised at 4.93, and *b* is 0.93±0.29. The square-shaped data show cumulative earthquake occurrences, whereas the red line indicates the linear fit of the frequency and magnitude distribution based on the Gutenberg-Richter equation.

An M_c value of 4.5 indicates that the earthquake catalogue is complete for earthquakes with magnitude of 4.5 or more. Furthermore, *a* value of 6.6 is associated with intense seismic activity in the region for small-to-large earthquakes. The *b*-value of 0.93±0.29 indicates a balanced trend between the large and small earthquakes. These average values of *a* and *b* correspond to the values in the Bird's Head of Papua Island in the eastern study area, including *a* = 7.09 and *b* = 0.92±0.02 (Lewerissa *et al*., 2021). This *b*-value, close to 1, indicates high stress in the study area, while the standard deviation of 0.29 shows variation in the estimated *b*-values but remains stable, providing high confidence in the calculation results. Mathematically, *a* is the log number of earthquakes with *M* = 0 and varies between 2 and 8, whereas *b* is the slope between the cumulative number and earthquake magnitude, ranging from 0.5 to 1.5. Different regions and scales depend on tectonics, structural heterogeneity, and stress distribution (Bora *et al*., 2018).

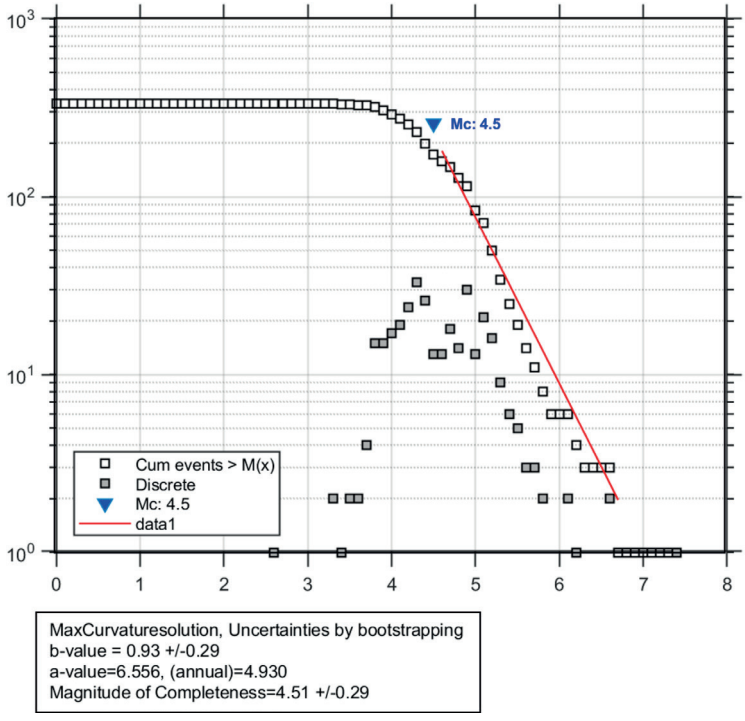

Fig. 9 - The FMD for the study area with a M_c value of 4.51±0.29, mean *a* value of 6.6, annual *a* of 4.93, and *b* value of 0.93±0.29.

We analysed the spatial distribution of seismicity parameters *a* and *b* and deviations of *b* in the Sorong fault zone. Fig. 10a shows values ranging from 4.60 to 8.40. Fig. 10b shows *b*-values ranging from 0.65 to 1.35, with standard deviations ranging from 0.05 to 0.32 (Fig. 10c). The *a* and *b* values exhibited a similar variation pattern, with high values dominating in the east and decreasing westwards. High standard deviations generally correspond to high *b*-values and vice

versa, with low-deviation areas showing consistent results, providing confidence in the estimated *b*-values in the Sorong fault zone region. Areas with higher standard deviations indicated greater variation in *the b*-values. This uncertainty may stem from geological heterogeneity or variations in the quality of seismic data. Higher *b*-values may be related to rocks with low strength that experience brittle cracking at lower-stress levels. High *b*-values may also indicate low stress levels in seismogenic zones owing to episodic changes in the tectonic linkage conditions (Sabahi *et al*., 2024). In the Sorong and neighbouring fault zones, *the b*-values are predominantly low to intermediate ($b \leq 1.0$), indicating that this region is mainly associated with thrust and strike-slip faults that experience higher stress regimes (Schorlemmer *et al*., 2005).

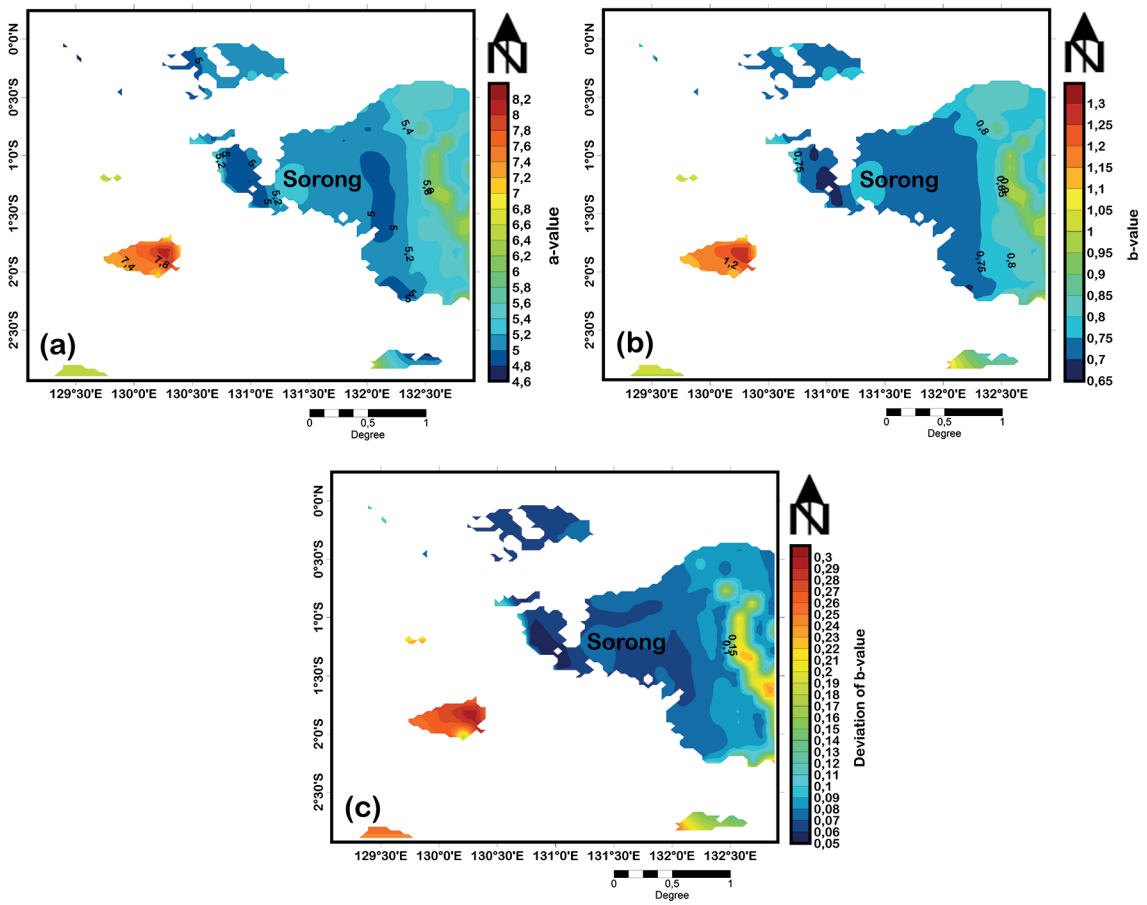

Fig. 10 - Spatial distribution of seismicity parameters in the Sorong fault zone in Bird's Head, Papua: a) *a*-value, b) *b*-value, and c) standard deviation of *b*-value.

4.2. Peak ground acceleration and spectral acceleration in the Dampier segment, Sorong fault zone

The *PGA* values in the Sorong fault zone area, particularly in the Dampier fault segment, based on the MPSHA approach, ranged from 0.016 to 0.265 g for a 50-year return period. The minimum *PGA* values indicate that the study area has the potential to experience relatively low

ground acceleration, which is typically associated with minor or distant earthquakes. Conversely, the maximum *PGA* values indicate the potential for major earthquakes likely originating near the primary earthquake source, such as the Dampier fault segment. *PGA* values vary with the spatial distribution of seismic hazards and are influenced by source distance, earthquake mechanism, and local geology. The seismic hazards at the study site are detailed using *Sa* values at vibration periods of 0.2, 0.3, 0.6, 1.0, and 2.0 s (Table 2).

Table 2 - Acceleration spectrum by period based on PSHA analysis in the Dampier segment of the Sorong fault zone.

Period (s)	S_a (g)	
	min	max
0.2	0.040	0.550
0.3	0.026	0.352
0.6	0.013	0.156
1.0	0.006	0.077
2.0	0.002	0.028

Sa is a ground motion parameter that accounts for sustained shock energy over a given period. Based on Table 2, the vibration periods can be classified into three categories: short (0.2-0.6 s), medium (1 s), and long (2 s). The *Sa* values are usually higher in the short period and show a consistent decline in the medium to long period. In the short period, seismic waves contributed significantly to the ground acceleration values.

In contrast, during medium and long periods, ground acceleration tends to be lower because the energy generated by the earthquake is relatively small. High *Sa* values in the short period, particularly between 0.2 and 0.3 s, indicate the potential for seismic wave amplification in shallow soil layers. Locations near the Dampier fault segment in the Sorong fault zone, which serves as the main earthquake source, are likely to experience a direct and intense impact of seismic waves owing to their proximity to the epicentre. Fig. 11a shows the *PGA* map of the Sorong area and its surroundings, which are adjacent to the Dampier fault segment. The maximum hazard zone, with a value of approximately 0.3 g, appeared semicircular around the fault, and the acceleration values decreased as the distance from the segment increased. This low *PGA* value is also believed to be related to the soil conditions in the study area based on the distribution of V_s-30, which is dominated by soft and stiff soils with low-to-moderate velocities.

Fig. 10 illustrates that high *PGA* values are frequently associated with low *b*-values in seismicity, indicating that the region under study is predominantly impacted by large-magnitude earthquakes. Figs. 11b to 11f show the acceleration spectrum maps for short to long periods, showing a pattern similar to the *PGA* maps in the study area. In the northern part, especially around the city of Sorong, consistently high values were observed on all the maps. In the central to southern regions, the indicated values ranged from medium to low, with a downward gradient pattern from NE (near active fault segments) to SW, indicating the dominant influence of the distance from the main earthquake source. In general, the *PGA* values obtained in this study are consistent with previous research on *PGA* at the regional level for the entire island of Papua, with values ranging from 0.06 g to 2.01 g, where the Sorong fault zone has *PGA* values smaller than 0.3 g (Makrup *et al*., 2018). In addition, the *PGA* values in our study are also consistent with

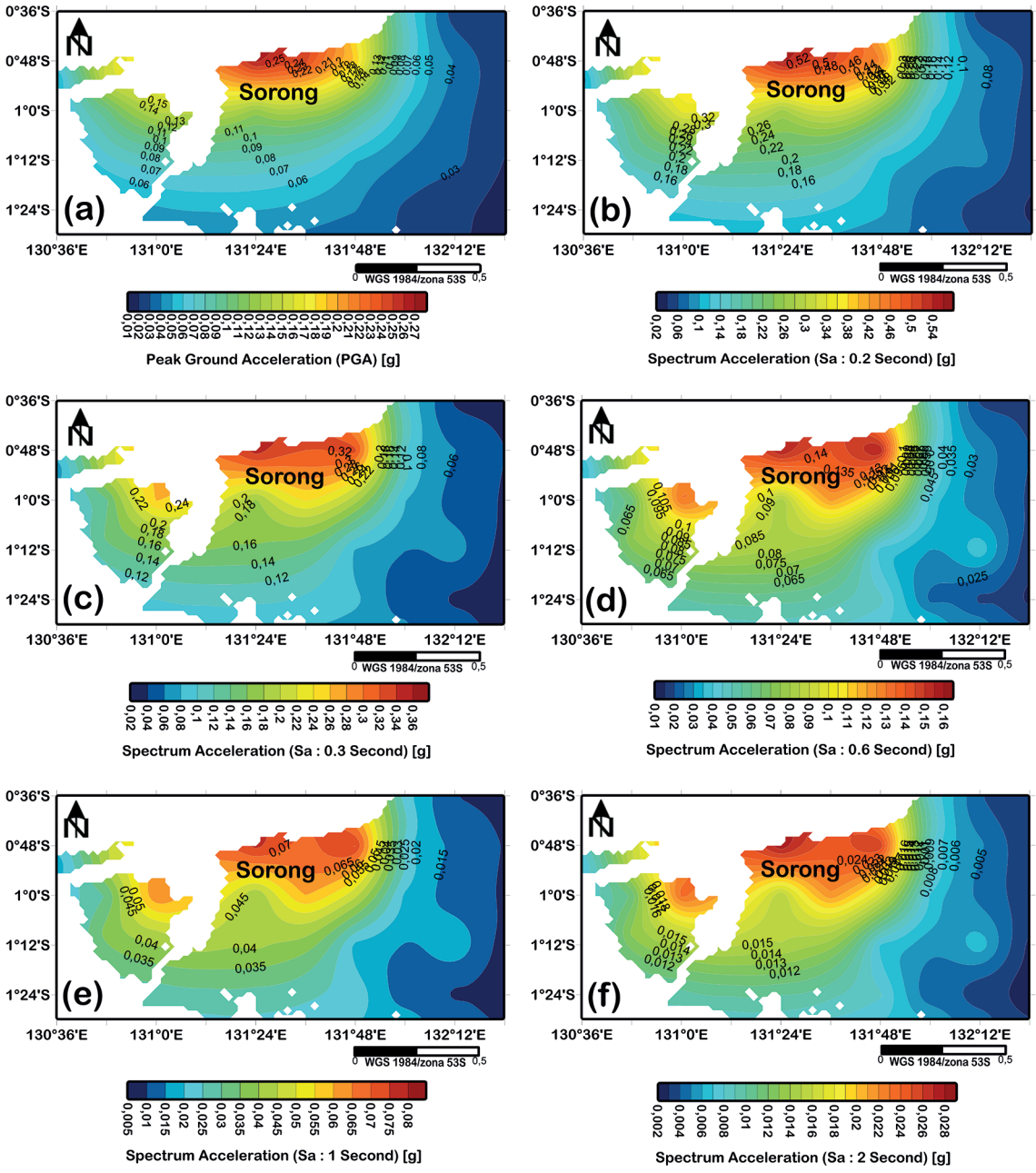

Fig. 11 - Seismic hazard maps near the Sorong strike-slip fault zone for a 50-year return period considering the specific local soil or rock conditions: a) average *PGA*; b) average *Sa* 0.2 s; c) average *Sa* 0.3 s; d) average *Sa* 0.6 s; e) average *Sa* 1.0 s; f) average Sa 2.0 s.

the Global Earthquake Model Global Seismic Hazard Map (version 2023.1), which depicts the geographical distribution of *PGA* with a 10% probability of exceedance over 50 years, ranging from 0.20 g to 0.35 g, using a V_s-30 of 760–800 m/s, shown in https://maps.openquake.org/map/gshm-2023-1/#7/-2.016/133.644 (Johnson *et al.*, 2023).

4.3. Depth of regional and residual gravity source in the Sorong fault zone

Subsequently, we analysed the WGM2012 gravity data to obtain preliminary information about the subsurface structure in the Sorong fault zone, which does not serve as a primary input parameter in the PSHA. This approach aims to enable the comparison and integration of seismic and gravity data at the interpretation stage, thereby enhancing the understanding of tectonics and earthquake hazard potential in the study area. This study involved three models: complete Bouguer anomaly, FA anomaly, and topography-bathymetry. The complete Bouguer anomaly of the Sorong region ranged from 160.15 to 316.40 mGal (Fig. 4a), whereas the FA anomaly ranged from -55.47 to 183.37 mGal (Fig. 4b). Topographic and bathymetric data from GEBCO_2024 cover heights from -2543 to 1131 m (Fig. 5).

High Bouguer anomalies dominate the north with a W-E orientation, which is related to the New Guinea Trough. Southwards, the Bouguer anomaly decreased, reaching its lowest value in the western region. The high Bouguer anomalies in this region are likely related to denser rock masses in the subsurface, where active subduction zones, such as the New Guinea Trough, support the intensity of seismic activity (Fig. 4b). FA anomalies show gravity field variations influenced by the surface topography and subsurface density. High FA anomalies were distributed in the southern part with a higher topography, whereas low FA anomalies dominated the northern oceanic region (Fig. 4a). The Bird's Head region shows steep relief and major elevation differences in topography and bathymetry (Fig. 4b). However, interpreting these features in terms of tectonic activity requires independent geophysical and geological evidence that falls outside the scope of this discussion on gravity anomalies.

We conducted a two-dimensional (2D) power spectrum analysis of the complete Bouguer anomaly data in the Bird's Head region of Papua on the Sorong fault line. The cut-off frequency divides the gravity data spectrum into low- and high-wavenumber domains. The high- and low-frequency domains correspond to shallow and deep sources, respectively, such as residual and regional anomalies (Maden and Elmas, 2022). The spectrum versus wavenumber graph shows straight-line sections with decreasing slopes as the frequency increases. These slopes provide information about the depths of the anomalous source at different levels. Analysis of the gravity anomaly spectrum over the Sorong fault zone revealed four signal groups representing specific source depths: deep sources, shallow sources, and noise (Fig. 12).

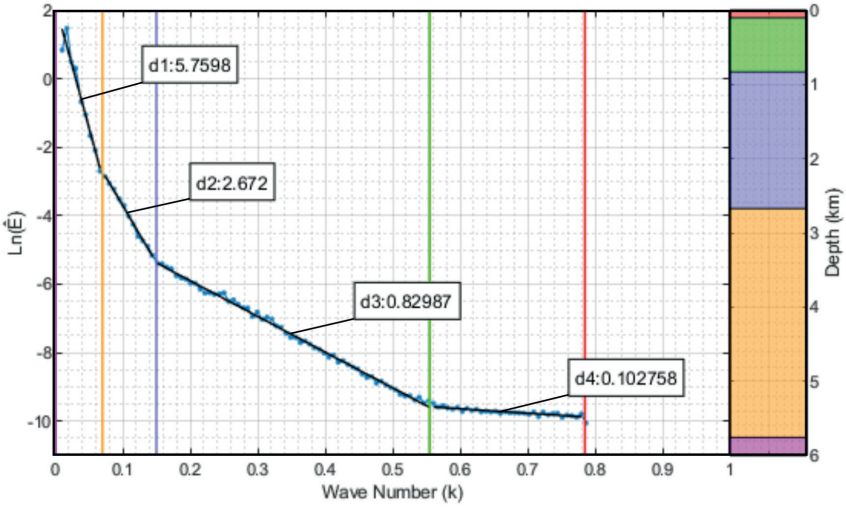

Fig. 12 - 2D Radial power spectrum of the complete Bouguer anomaly in the Bird's Head region of Papua in the Sorong fault zone.

The slopes of the signals were identified using linear regression. The low wavelength signal indicates that the top depth reaches 5.76 km (d_1), which is related to a deep or basement source. A shallow source was identified from the second line slope with an upper depth of 2.7 km (d_2), associated with thick sediments at the basement boundary. The third slope corresponds to a shallower source with a layer depth of 0.83 km (d_3). The fourth slope and beyond are horizontal and relate to gravity anomaly data noise (d_4). Analysis of gravity data revealed spectral variations between shallow and deep sources, indicating distinct differentiation in the rheology of the deep and shallow crust. Consequently, these two zones exhibit different mechanical behaviours. This radial power spectrum analysis serves as a reference for separating regional and residual gravity anomalies using upward continuation (UC) in the Bird's Head region of Papua in the Sorong fault zone. To characterise the Sorong fault zone, the ED method was first applied to the Bouguer anomaly data for this location. The ED technique interprets geophysical parameters such as anomaly source depth and subsurface structure. ED analysis in the horizontal plane maps fault geometries and lithologic patterns linked to rock density variations (Chen *et al*., 2014). The Bouguer anomaly in the Sorong fault zone shows variations that reflect subsurface rock density heterogeneity. The pattern shows high gradients in the fault trend direction, indicating density contrasts owing to tectonic movements and deep structures.

Two cross-sections (A-B and C-D) were positioned perpendicular to the fault to isolate the gravity response from the complex subsurface structure (Fig. 13a). The 3D ED solution, with N = 1 for contacts or faults, showed clusters concentrated along the Sorong fault zone. This cluster represents an anomaly source dominated by vertical structures that match the Sorong shear fault model. The depth varies between 500 and 12000 m, indicating variations in the fault geometry or nearby secondary structures (Fig. 13b). To confirm the 3D ED solution, we analysed the 2D ED for cross-sections A-B and C-D, which were cut perpendicular to the fault zone. In cross-section A-B (length ±100 km), the 2D Euler solution confirmed an anomalous source with a maximum depth greater than 10 km below the surface. The solution points formed a linear pattern parallel to the Sorong fault surface projection at an average depth of ~6 km. A consistent N = 1 indicates that the vertical contact (fault) source model is more dominant than the other models (Fig. 13c). Cross-section C-D (length ±100 km) shows a solution with a maximum depth up to 15 km deeper than cross-section A-B. This difference may reflect variations in fault geometry or the influence of local structures such as small fault zones or deformed sedimentary rocks. The dispersed solution clusters in this incision suggest structural complexity in the eastern study zone (Fig. 13d).

In this study, the ED analysis was used to estimate the depth and initial shape of the anomaly source, together with 2D radial power spectrum analysis. This is due to the possibility that the 3D results in Fig. 13b do not fully reflect the actual conditions, but, instead, only provide a rough estimate of the location of the top edges of the anomaly source in the Sorong fault zone because of their non-unique nature and sensitivity to the selection of parameters such as structural index, window size, and grid resolution. In addition, 2D ED was intended to further emphasise the results obtained from the 3D ED analysis.

4.4. Regional and residual gravity anomalies in the Sorong fault zone

In this study, regional and residual gravity anomalies were separated using the UC method at an elevation of 6000 m. The selection of this elevation was based on the wavelength approaching the spectral transition point from the results of the 2D radial power spectrum analysis (Fig. 12) and the ED analysis (Fig. 13) from the complete Bouguer anomaly data of the Sorong fault zone,

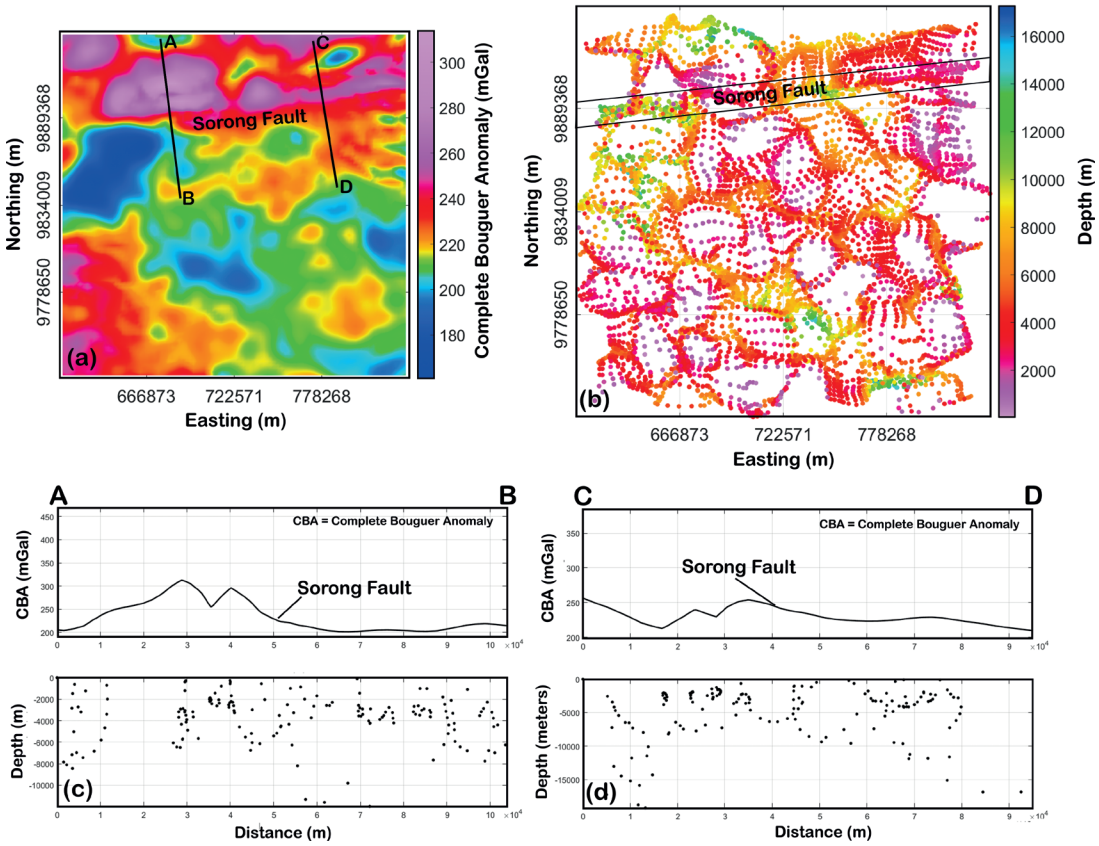

Fig. 13 - ED analysis of the Sorong fault zone and surrounding area: a) complete Bouguer anomaly as input and two transverse cross-sections perpendicular to the Sorong fault; b) 3D ED solution with N = 1, focused on the Sorong fault zone, which extends from west to east; c) 2D ED solution of cross-section A-B with N = 1; d) 2D ED solution of cross-section C-D with N = 1.

which illustrates the difference between shallow and deep anomaly sources. Although frequency-based filtering methods in the wavenumber domain can provide more precise frequency control, UC was chosen because it is relatively easy to implement and is more resistant to noise amplification, which can sometimes occur with high-pass filtering in the spectral domain. Thus, this approach is consistent with the results of spectral analysis while maintaining data stability during the anomaly separation process. The continuation occurred at 1000 m (Figs. 14a and 14b), 3000 m (Figs. 14c and 14d), and 6000 m (Figs. 14e and 14f). The 6000 m UC served as the reference level for differentiating regional and residual components because of its effectiveness in highlighting residual anomalies linked to the Sorong fault. Similar to 1000 m and 3000 m continuations, it places less emphasis on higher-frequency elements, likely from data noise.

The regional anomaly at 6000 m ranges from 185 to 275 mGal, with high values in the north decreasing southwards. The regional anomaly shows high values in the NW and decreasing values in the SW of the study area (Fig. 14e). Regional gravity anomalies are associated with broad, deep geological structures dominated by igneous or volcanic rocks. The residual gravity anomaly is the difference between the complete Bouguer anomaly and the regional anomaly from the UC at 6000 m. The residual anomaly ranged from -35 to 50 mGal, with positive anomalies in the north decreasing to negative anomalies in the south (Fig. 14f).

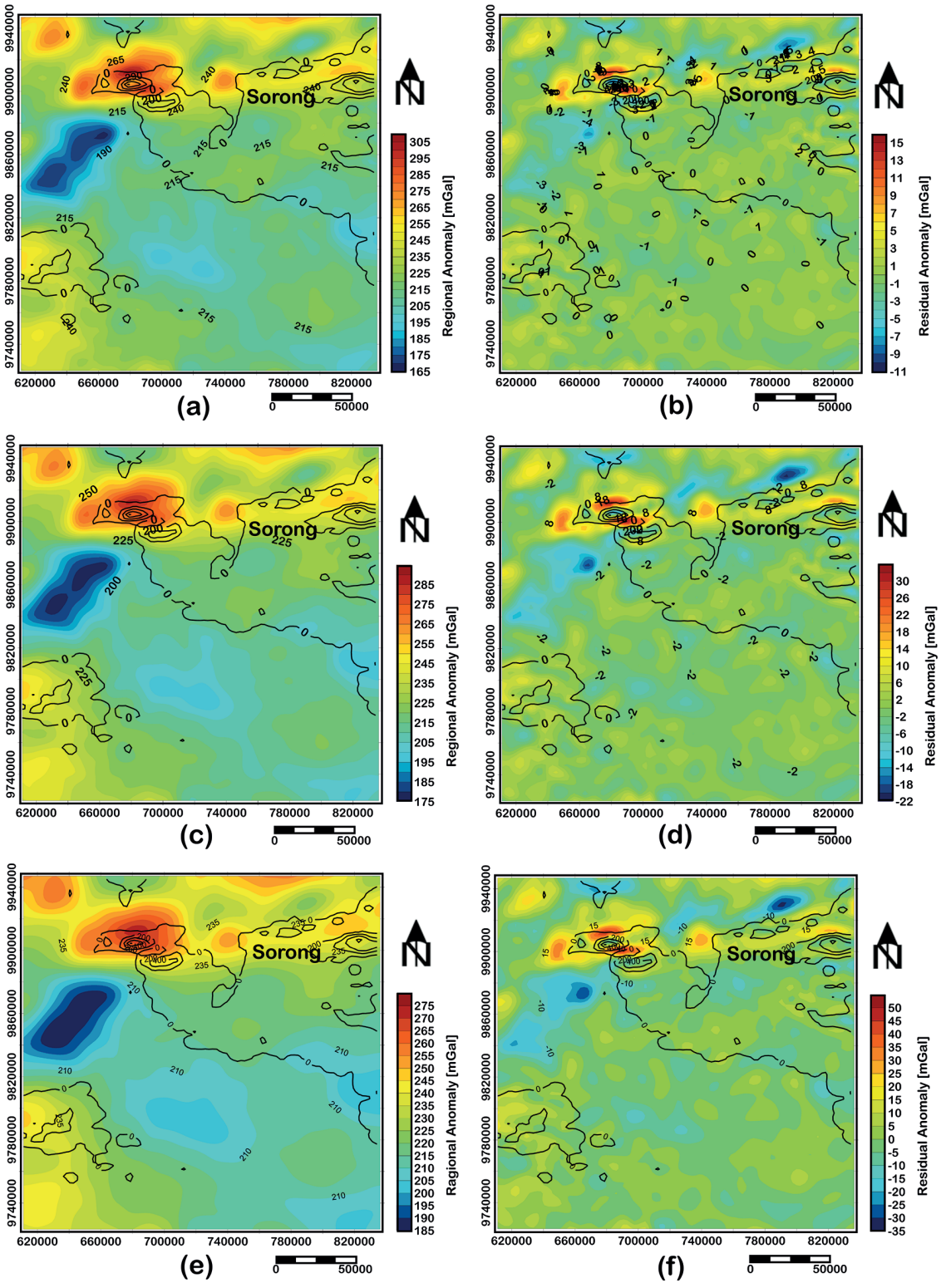

Fig. 14 - Separation of regional and residual gravity anomalies through UC at various heights: a) 1000 m regional anomaly, b) 1000 m residual anomaly, c) 3000 m regional anomaly, d) 3000 m residual anomaly, e) 6000 m regional anomaly, and f) 6000 m residual anomaly.

The residual gravity anomaly pattern is more complex than the regional anomaly but follows the complete Bouguer anomaly pattern. Gravity anomalies are related to near-surface geological structures that are generally complex. Negative gravity anomalies likely occur because the rocks are fractured owing to intense tectonic activity in the study area. The Sorong fault zone has a W-E direction and exhibits high-gravity regional and residual anomalies in each separation. The Sorong fault zone serves as a magmatic conduit.

The Berangan Andesite volcanic formation, formed after the Pliocene, lies north of the main Sorong fault zone and is likely to have used this zone as a conduit for surface eruptions. The Sorong fault zone acts as a magma conduit, leading to crustal contamination, as evidenced by the geochemical data and inherited zircons from the Berangan Andesite (Webb *et al*., 2020). Magmatic activity affects the rock density distribution in the subsurface, as indicated by gravity anomalies. Positive gravity anomalies near the Sorong fault zone indicate magma intrusions or igneous rocks with higher densities than the surrounding rocks. Negative gravity anomalies occur where voids or altered rocks have lower densities owing to magmatic processes. The residual anomaly data at 6000 m UC altitude served as input for the gravity anomaly inversion modelling of the Bird's Head region in the Sorong fault zone.

4.5. Subsurface model of the Bird's Head region of Papua at the Sorong fault zone

The inversion process begins with forward modelling to calculate the gravity anomaly based on an initial model with a constant density. The model was adjusted iteratively to minimise the differences between the observed anomalies and calculated results. The inversion was performed until the difference between the observational data and the model fell below the convergence threshold. In this study, the maximum number of iterations was set to 50, with a convergence criterion of root-mean-square error <5%. Density constraints were applied between 2.0 g/cm^3 and 3.5 g/cm^3 to ensure geologically consistent results. The application of these physical constraints was intended to reduce the non-uniqueness of the gravity inversion and improve the stability of the final model (Li and Oldenburg, 1996).

Fig. 15a shows the observation data as residual anomaly values at an altitude of 6000 m, ranging from -35 to 50 mGal. Iterations were performed to produce calculation data that reflected the anomaly pattern with values close to those of observational data (Fig. 15b). The accuracy was confirmed by the small difference value, which showed a high match between the observed and computed data after inversion (Fig. 15c). The modelling error was 4.5%. Five cross-sections, that cut seven faults in the study area, were obtained. They are shown in 2D form to clarify the earthquake faults causing earthquakes in Sorong and its surroundings. Gravity inversion modelling produced a 3D subsurface density distribution model in the Bird's Head region of Papua on the Sorong fault line (Fig. 16).

The correspondence between the observed gravity anomalies and calculated results indicates that the inversion model can accurately reproduce the gravity signals in the North Kofiau segment (Fig. 17a). However, this does not directly validate the subsurface geological density distribution of the Sorong fault zone. Given the non-unique nature of gravity inversion, we consider the resulting model to be a possible subsurface model that fits the data. Fig. 17b shows the distribution of subsurface rock density with depth, with density variations primarily observed along the Sorong fault line in the North Kofiau segment. Rock densities range from low (approximately 2.2 g/cm^3) to high (approximately 3.0 g/cm^3), reflecting differences in composition and the potential occurrence of rock deformation. High-density zones are suspected to correlate with bedrock or magmatic intrusions, whereas low-density zones may indicate rock deformation due to fault activity.

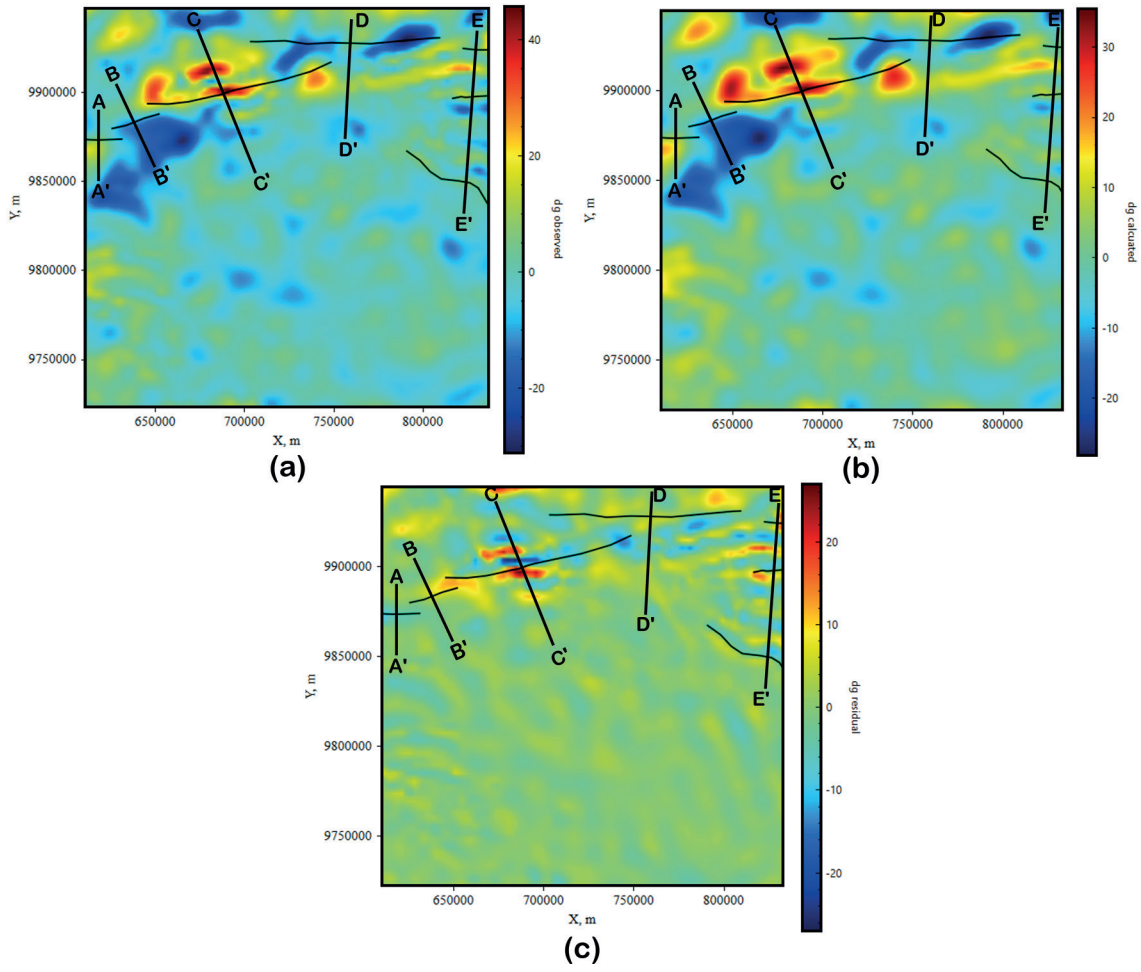

Fig. 15 - Results of 3D inversion modelling of 6000 m residual gravity anomaly: a) observation data, b) calculated data, and c) difference data.

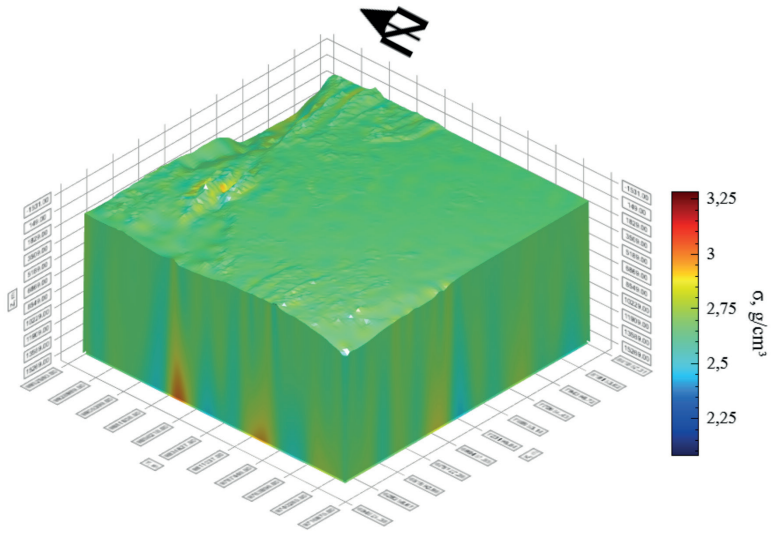

Fig. 16 - 3D model of rock density distribution in the Bird's Head region of Papua in the Sorong fault zone based on gravity anomaly inversion modelling.

Variations in the density of the Sorong fault zone in the North Kofiau segment are suspected to be related to the complexity of geological structures. Our hypothesis suggests that low-density zones may result from deformation processes that commonly occur in active fault zones. In addition, the high density in certain locations may be associated with the presence of more volcanic rocks or magmatic intrusions (Fig. 1), which can influence fault movement mechanisms and the accumulation of tectonic stress in this segment. Low-density zones along the Sorong fault in the North Kofiau segment may be more susceptible to fault movement and could serve as sources of seismic-energy release.

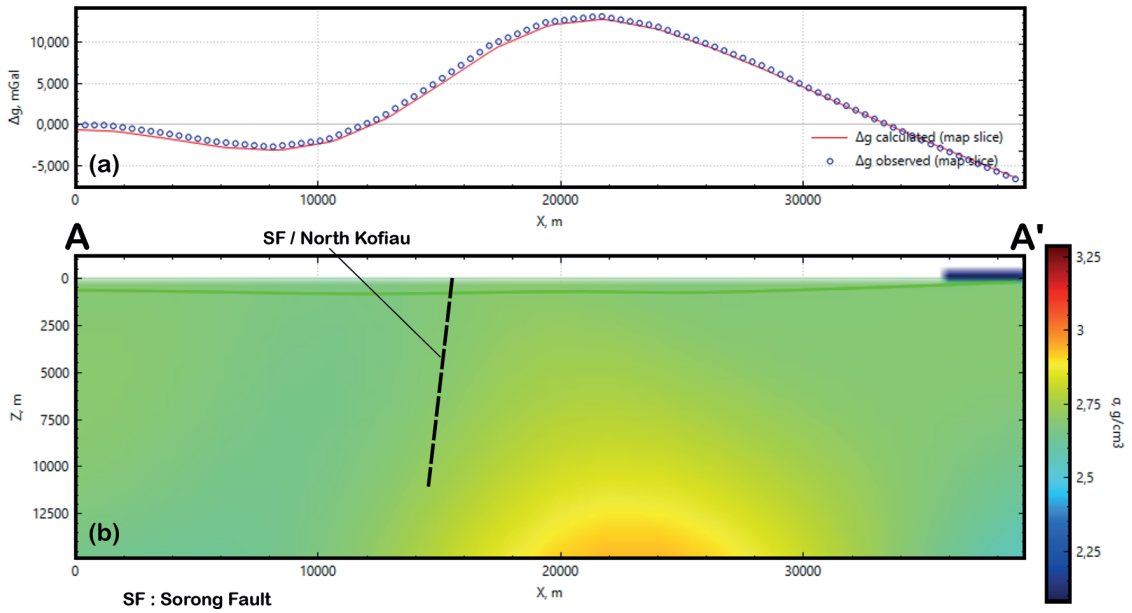

Fig. 17 - The 2D A-A' cross-section intersects the Sorong fault, with a dashed line marking the boundary of the North Kofiau segment: a) alignment between the observed and calculated gravity anomaly data; b) model fit for subsurface rock density variation distribution with depth.

Fig. 18a illustrates the correlation between the observed gravity anomalies and the calculated results, demonstrating that the inversion model accurately replicated the gravity signals in the West Salawati segment. Similar to the inversion results from the northern Kofiau segment, these findings do not directly confirm the subsurface geological density distribution of western Salawati. We regard the resulting model as a potential subsurface model that aligns with the data, considering the inherent ambiguity of gravity inversion.

Fig. 18b shows the distribution of subsurface rock density with depth, where variations in density are evident in this segment. Rock density ranges from low to high, between 2.2 and 3.0 g/cm^3, which is likely related to differences in composition and the presence of rock deformation. High-density zones may correlate with magmatic intrusions in the northern part of this segment (dashed line), whereas low-density zones at a depth of 12 km may indicate sedimentary rocks deformed by fault activity in the southern West Salawati segment. The interpretation of this low-density zone is assumed to be an initial hypothesis that requires confirmation from other geological or geophysical data. Compared with North Kofiau, the West Salawati segment showed smaller variations in rock density.

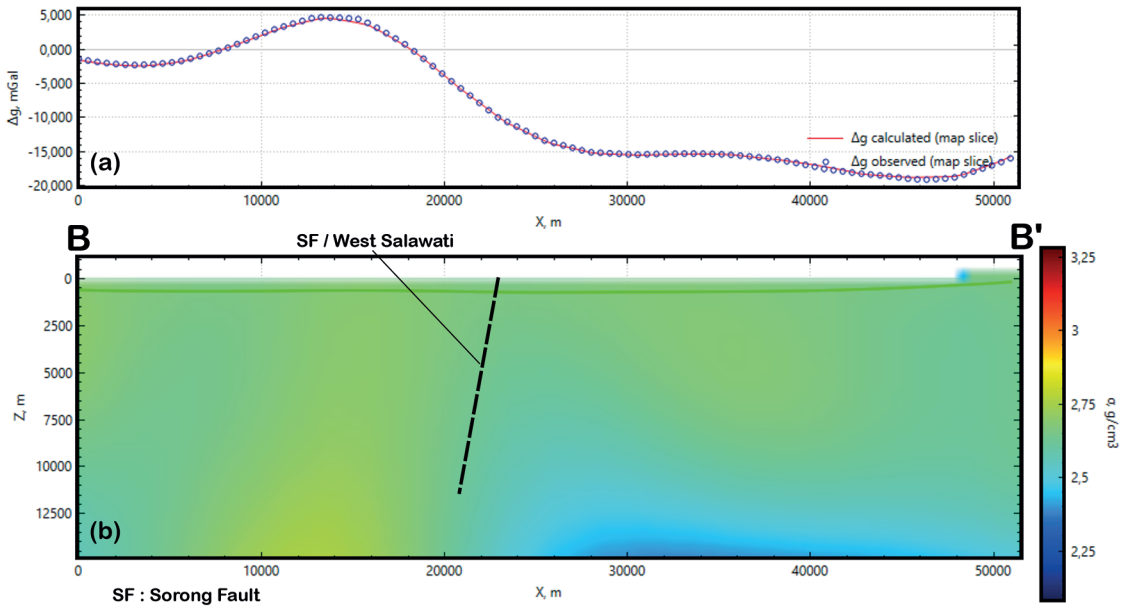

Fig. 18 - The 2D B-B' cross-section intersects the Sorong fault, with a dashed line marking the boundary of the West Salawati segment: a) alignment between the observed and calculated gravity anomaly data; b) model fit for the subsurface rock density variation distribution with depth.

Fig. 19a shows the correspondence between the observed and calculated gravity anomaly data along the C-C' cross-section of the Sorong fault zone in the Sagewin segment. This correspondence confirms that the resulting model can represent the subsurface density distribution with a gravity anomaly curve that is more complex than that of the previous two segments. Fig. 19b shows a 2D cross-section that reveals significant lateral density variation along the profile. A low-density anomaly (indicated in blue) is adjacent to a high-density zone (indicated in red) approximately 40 km along the cross-section. This striking density contrast coincides with the interpreted location of the Sorong fault in the Sagewin segment, indicating the presence of a major lithological boundary or a significant deformation zone. The fault appears as an almost vertical structure cutting through the crust, which is consistent with the characteristics of strike-slip fault systems.

The observed density contrast suggests the displacement of different crustal blocks, likely due to ongoing tectonic activity. The high-density zone likely reflects the presence of basement rocks or intrusive bodies, whereas the low-density zone indicates an area that has been intensely fractured or filled with material owing to fault activity. The presence of low-density zones may be associated with areas of the crust that have undergone weakening, possibly due to fluid infiltration, given the fault's length in the sea, which reaches 125 km (Table 1) and the potential existence of extensive fractures. This condition may serve as an area of stress accumulation, thereby increasing the likelihood of future seismic activities.

Fig. 20a shows the correspondence between the observed gravity anomaly data and the calculated results along the Sorong fault and Dampier segment. This result is also considered as a model that can represent the subsurface density distribution in that segment. Fig. 20b shows the subsurface density distribution obtained from 3D gravity inversion. In general, this model demonstrates the dominance of rocks with relatively homogeneous density in most areas, with values ranging from 2.5 to 2.75 g/cm^3, which are likely associated with sedimentary or metamorphic rocks with low lithological differentiation. The presence of fault structures is

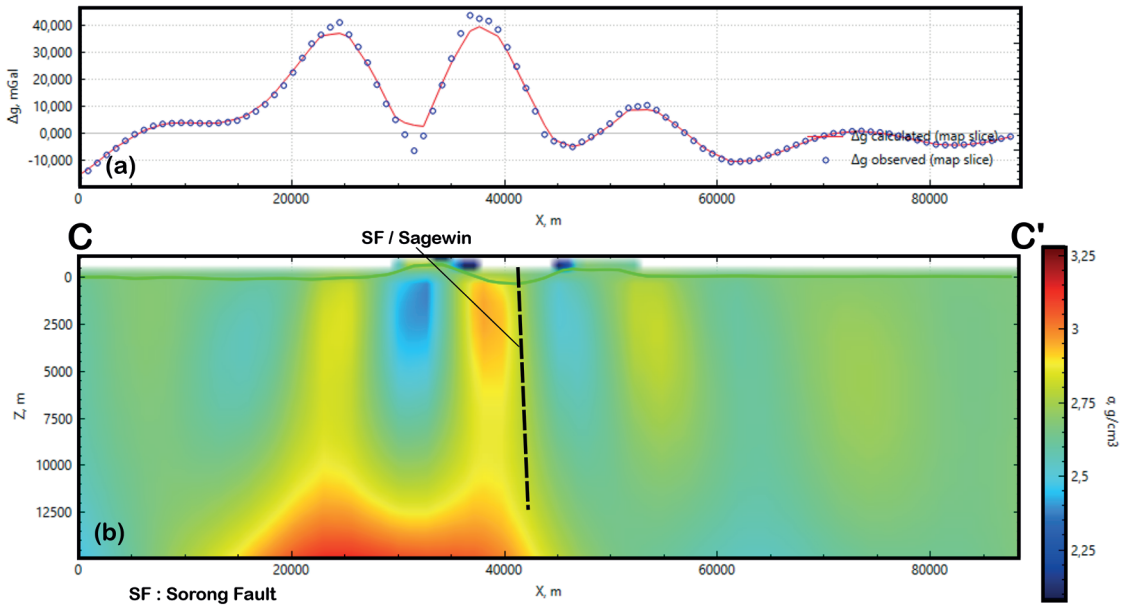

Fig. 19 - The 2D C-C' cross-section intersects the Sorong fault, with a dashed line marking the boundary of the Sagewin segment: a) alignment between the observed and calculated gravity anomaly data; b) model fit for the subsurface rock density variation distribution with depth.

indicated by discontinuity planes (dashed black lines) that cut across the surfaces. Compared with the Sagewin segment (Fig. 19), the Dampier segment did not show significant lateral density contrast.

This suggests that in this segment, the fault may not extend to greater depths or that the fault zone has been refilled with material of uniform density. The zone with a lower density (yellow to light green) at the bottom of the model may indicate a zone of weakening due to tectonic activity or the intrusion of lighter material. Without significant indications of high density, the hypothesis of the presence of intrusive igneous rocks in this segment requires further study because it is also located at sea. The interpreted fault structure in the Dampier segment showed a steeper dip and was not as deep as that in the Sagewin segment. This indicates that tectonic movement in this segment is dominated by the reactivation of faults in shallow layers rather than deformation affecting deeper layers. In general, the subsurface model from gravity modelling shows correspondence with the distribution of hypocentres depicted in Fig. 2 in the Sorong fault zone, particularly in the western Dampier segment.

Fig. 21a shows the correspondence between the observed gravity anomaly data and the calculations from the inversion modelling along the E-E' line, covering the Mega Omnowi, Klararea, and South TT segments. The similarity in the anomaly patterns indicates that the inversion model is reliable in representing the subsurface density distribution with good accuracy. Fig. 21b shows the subsurface density distribution with complex lateral variations, particularly in the main fault zones. Low-density zones (green-yellow colour) were distributed at intermediate to greater depths, whereas high-density zones (blue colour) were found closer to the surface. The Sorong fault in the Mega Omnowi and Klararea segments is marked by a density discontinuity at depths greater than 5,000 m. The lateral density differences in this zone indicate the presence of fractures or different rock materials along the fault line. Tectonic activity along this segment plays a role in the deformation of the Earth's crust. The southern

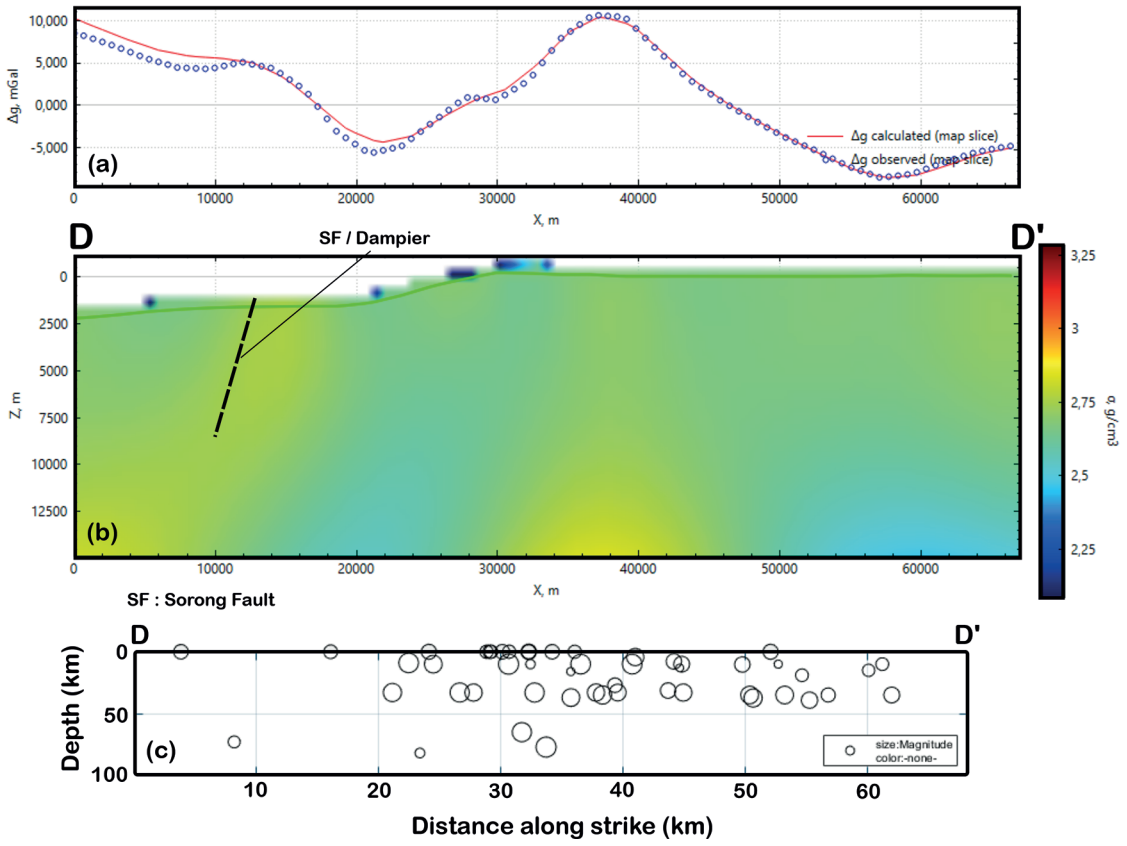

Fig. 20 - The 2D D-D' cross-section intersects the Sorong fault, with a dashed line marking the boundary of the West Dampier segment: a) alignment between the observed and calculated gravity anomaly data; b) model fit for the subsurface rock density variation distribution with depth; c) distribution of earthquake hypocentres based on Fig. 2 along the D-D' cross-section of the West Dampier segment.

TT shows a southward dip with a more heterogeneous density and has the potential to be a boundary between two crustal blocks with different lithologies. The presence of faults and thrusts indicates highly complex tectonic deformation. From a seismic hazard perspective, low-density zones around the fault line can indicate zones of crustal weakening that have the potential to become sites of stress concentrations and seismic energy accumulation. The thrust identified in the southern part can increase the complexity of regional stress and is often associated with large-magnitude earthquakes owing to its compressional mechanism, which stores energy before it is released.

Based on Figs. 16 to 21, several zones with high rock densities exist, particularly in some segments of the Sorong fault. This high rock density is believed to be related to the geology of the volcanic rocks, specifically the Auwewa and Dore volcanics. Conversely, zones with low rock densities are thought to be associated with fault zones and fractures resulting from intense deformation in this area. The Auwewa volcanic group consists of volcanic rocks formed during the Oligocene period, including the Mandi, Arfak, and Dore Volcanics. This group was formed during the northward subduction of the Australian plate beneath the Philippine Sea plate. Specifically, the Dore Volcanics is one of the units located in the north-western part of Bird's Head of Papua, which is exposed north of the Sorong fault zone (Webb *et al*., 2020).

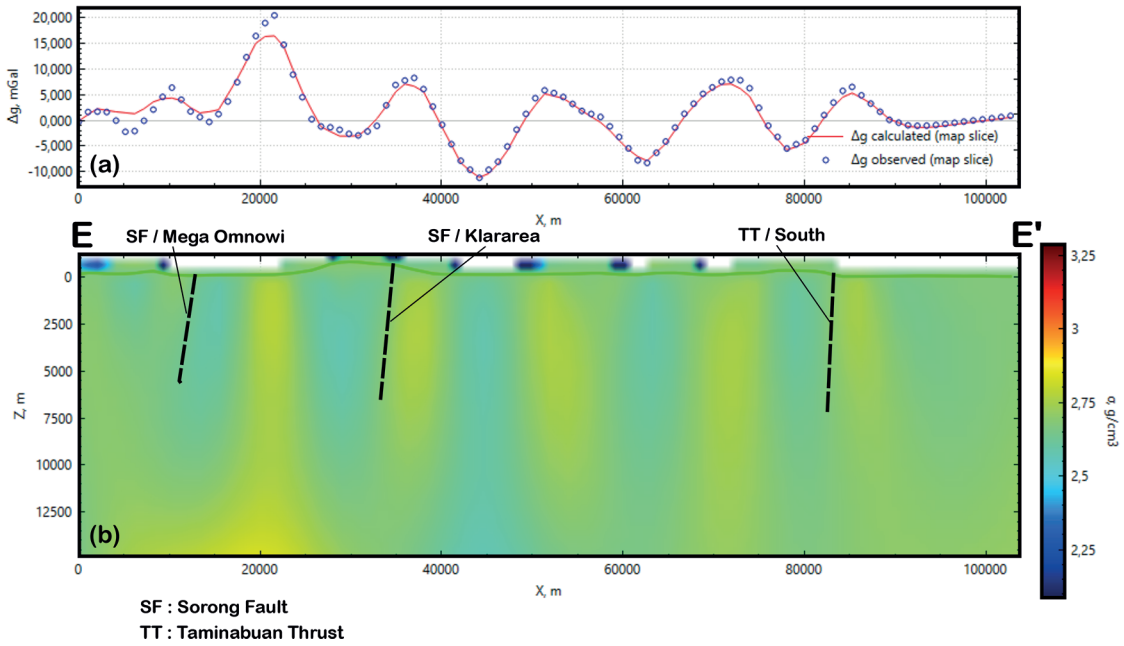

Fig. 21 - The 2D E-E' cross-section intersects the Sorong fault, with the dashed line indicating the boundary between the Mega Omnowi and Klararea segments and the South TT: a) alignment between the observed and calculated gravity anomaly data; b) model fit for the distribution of subsurface rock density variation with depth.

The Dore Volcanics are characterised by lava, lava breccia, tuff, and volcaniclastic rocks with andesitic to basaltic compositions. In addition, this unit contains small diorite intrusions, with some samples showing high potassium calc-alkaline (high-K) to shoshonitic characteristics. The Dore Volcanics is a volcanic unit bounded by faults that shows a close spatial relationship with the Sorong fault system. This is evidenced by the presence of extensive fault and fracture structures, indicating oblique dip-slip and sinistral strike-slip movements. Volcanic rocks, such as andesite and basalt, generally have high densities. In addition, the presence of small diorite intrusions adds to the complexity of rock density, as diorite has a higher density than the surrounding rocks.

5. Conclusions

This study combined seismological and gravity analyses to understand the tectonic characteristics and seismic hazard potential of the Sorong fault zone on Papua Island. Seismic analysis describes the distribution of earthquake activity, source characteristics, and hazard estimates using PSHA, including *PGA* and *Sa*. Gravity data analysis, which includes the radial power spectrum, ED, regional-residual anomaly separation, and 3D gravity data inversion modelling, shows density contrasts that generally align with the fault path and its related segments. Analysis of gravity data revealed spectral variations between shallow and deep sources, indicating distinct differentiation in the rheology of the deep and shallow crust. Consequently, these two zones exhibit different mechanical behaviours. Overall, the spatial correlation between anomalous or density-gradient zones and seismicity concentrations supports the existence of active structures that are important for hazard assessment in this study area. Nevertheless, the results of gravity

analysis remain a preliminary framework owing to the non-unique nature and vertical resolution limitations of this method. The ED solution is considered an initial indication of the anomaly source location, not a definitive 3D boundary, and is sensitive to the choice of structural index, window size, and grid resolution. The 3D inversion results revealed areas of high or low density, which may indicate the presence of intrusions, shear zones, or deformed rocks. However, these findings are regarded as initial hypotheses that require further testing in future studies. The integration of these two methods may have implications for increasing the focus on priority mitigation areas around fault segments that exhibit a correlation between gravity anomalies and seismic hazard levels in the study area. To improve the accuracy of the interpretation and reliability of the model, further studies are recommended to strengthen the scientific basis for seismic hazard assessment and mitigation planning in Papua.

Acknowledgments. We thank the University of Papua for providing the opportunity to participate in the KTI Research Grant (Contract Number: SP-30b/UN42.15/PG/2024). We also thank the providers of the earthquake data from IRIS DMC and WGM 2012 Earth gravity data, which were used for further processing and analysis in this study. We also acknowledge the utilisation of open-source software such as Gravpack and Gravmag Suite, as well as the z-map used for data processing in this study. Data can be obtained upon request and with the consent of all authors.

REFERENCES

Ali M., Decarlis A., Geng M., Bosworth W., Ball P.J., Ligi M. and Ceriani A.; 2024: *Imaging Pleistocene volcanic edifices along the Egyptian Red Sea margin: insights from reflection seismics and 3D constrained inversion of gravity and magnetic data*. J. Volcanol. Geotherm. Res., 448, 108038, doi: 10.1016/j.jvolgeores.2024.108038.

Ali S.M. and Akkoyunlu M.F.; 2022: *Statistical analysis of earthquake catalogs for seismic hazard studies around the Karliova Triple Junction (eastern Turkey).* J. Afr. Earth Sci., 186, 104436, doi: 10.1016/j.jafrearsci.2021.104436.

Allen T.I. and Wald D.J.; 2009: *On the use of high-resolution topographic data as a proxy for seismic site conditions (VS30).* Bull. Seismol. Soc. Am., 99, 935-943, doi: 10.1785/0120080255.

Amri C.H., Sanyoto P., Harahap B.H., Supriatna S.S., Simanjuntak W. and Pieters P.E.; 1990: *Peta Geologi Lembar Sorong, Skala 1:250 000*. Pusat Survei Geologi, Bandung, Indonesia.

Aydın N.G. and İşseven T.; 2021: *GravPack: a MATLAB-based gravity data processing package.* Arabian J. Geosci., 14, 268, doi: 10.1007/s12517-021-06656-9.

Azizi M. and Saffari H.; 2024: *Spatial and temporal variation of seismic b-values across the west Tehran.* J. Seismol., 28, 477-489, doi: 10.1007/s10950-024-10196-6.

Badreldin H., ElHadidy M., Abu El-Ata A., Lala A.M. and Abd El-Aal A.E.-A.K.; 2024: *Site-specific probabilistic seismic hazard analysis in Nuweiba, Gulf of Aqaba, Egypt: combining area source model and active faults.* J. Afr. Earth Sci., 215, doi: 10.1016/j.jafrearsci.2024.105290.

Balmino G., Vales N., Bonvalot S. and Briais A.; 2012: *Spherical harmonic modelling to ultra-high degree of Bouguer and isostatic anomalies.* J. Geod., 86, 499-520, doi: 10.1007/s00190-011-0533-4.

Benali A., Jalilian A., Peresan A., Varini E. and Idrissou S.; 2023: *Spatiotemporal analysis of the background seismicity identified by different declustering methods in northern Algeria and its vicinity.* Axioms, 12, 237, doi: 10.3390/axioms12030237.

Bencharef M.H., Boubaya D., Aboud E. and Ayfer S.; 2022: *Role of an advanced gravity data analysis in improving the geologic understanding of the northern Tebessa region, northeastern Algeria.* J. Afr. Earth Sci., 196, 104693, doi: 10.1016/j.jafrearsci.2022.104693.

Bora D.K., Borah K., Mahanta R. and Borgohain J.M.; 2018: *Seismic b-values and its correlation with seismic moment and Bouguer gravity anomaly over Indo-Burma ranges of northeast India: tectonic implications.* Tectonophys., 728, 130-141, doi: 10.1016/j.tecto.2018.01.001.

Castro F.R., Oliveira S.P., De Souza J. and Ferreira F.J.F.; 2018: *GRAV-MAG SUITE – An open source MATLAB-based program for processing potential field data.* In: Proc. VIII Simpósio Brasileiro e Geofísica, Salinópolis, PA, Brazil, 6 pp., doi: 10.22564/8simbgf2018.067.

Cauzzi C., Faccioli E., Vanini M. and Bianchini A.; 2015: *Updated predictive equations for broadband (0.01-10 s) horizontal response spectra and peak ground motions, based on a global dataset of digital acceleration records.* Bull. Earthquake Eng., 13, 1587-1612, doi: 10.1007/s10518-014-9685-y.

Chen Q., Dong Y., Cheng S., Han L., Xu H. and Chen H.; 2014: *Interpretation of fault system in the Tana Sag, Kenya, using edge recognition techniques and Euler deconvolution.* J. Appl. Geophys., 109, 150-161, doi: 10.1016/j.jappgeo.2014.07.020.

Chepigo L.; 2023: *GravMagInv3D - manual.* Moscow State University, Moscow, URSS.

Chiba K.; 2024: *Spatiotemporal variations in seismic activity in and around the focal region of the 2021 M7.3 and 2022 M7.4 Fukushima-Oki earthquakes, Japan.* Tectonophys., 870, 230150, doi: 10.1016/j.tecto.2023.230150.

Chioccarelli E., Cito P., Iervolino I. and Giorgio M.; 2019: *REASSESS V2.0: software for single- and multi-site probabilistic seismic hazard analysis.* Bull. Earthquake Eng., 17, 1769-1793, doi: 10.1007/s10518-018-00531-x.

Damanik R., Gunawan E., Widiyantoro S., Supendi P., Atmaja F.W., Ardianto A., Husni Y.M., Zulfakriza Z. and Sahara D.P.; 2023: *New assessment of the probabilistic seismic hazard analysis for the Greater Jakarta area, Indonesia.* Geomatics Nat. Hazards Risk, 14, 2202805, doi: 10.1080/19475705.2023.2202805.

De Lima D.P.D., Carmelo A.C., Soares J.E.P., De Lima M.V.A.G. and Fuck R.A.; 2023: *Gravity inversion for crustal thickness investigation of the continental and oceanic crusts of Brazil incorporating a lithosphere thermal gravity anomaly correction.* Tectonophys., 846, 229663, doi: 10.1016/j.tecto.2022.229663.

Di Giacomo D., Bondár I., Storchak D.A., Engdahl E.R., Bormann P. and Harris J.; 2015: *ISC-GEM: global instrumental earthquake catalogue (1900-2009), III. Re-computed M and m, proxy M, final magnitude composition and completeness assessment.* Phys. Earth Planet. Inter., 239, 33-47, doi: 10.1016/j.pepi.2014.06.005.

Eldosouky A.M. and Saada S.A.; 2020: *Source edge detection (SED) of aeromagnetic data: synthetic examples and a case study from Haimur area, south-eastern Desert, Egypt.* Arabian J. Geosci., 13, 626, doi: 10.1007/s12517-020-05653-8.

Essa K.S., Géraud Y. and Diraison M.; 2021: *Fault parameters assessment from the gravity data profiles applying the global particle swarm optimization.* J. Pet. Sci. Eng., 207, 109129, doi: 10.1016/j.petrol.2021.109129.

Gerstenberger M.C., Marzocchi W., Allen T., Pagani M., Adams J., Danciu L., Field E.H., Fujiwara H., Luco N., Ma K.-F., Meletti C. and Petersen M.D.; 2020: *Probabilistic seismic hazard analysis at regional and national scales: state of the art and future challenges.* Rev. Geophys., 58, doi: 10.1029/2019RG000653.

Ghasemi H., Cummins P., Weatherill G., McKee C., Hazelwood M. and Allen T.; 2020: *Seismotectonic model and probabilistic seismic hazard assessment for Papua New Guinea.* Bull. Earthquake Eng., 18, 6571-6605, doi: 10.1007/s10518-020-00966-1.

Gregori S.D. and Christiansen R.; 2018: *Seismic hazard analysis for central-western Argentina.* Geod. Geodyn., 9, 25-33, doi: 10.1016/j.geog.2017.07.006.

Hussain H., Shuangxi Z., Usman M. and Abid M.; 2020: *Spatial variation of b-values and their relationship with the fault blocks in the western part of the Tibetan plateau and its surrounding areas.* Entropy, 22, 1016, doi: 10.3390/e22091016.

Hutchings S.J. and Mooney W.D.; 2021: *The seismicity of Indonesia and tectonic implications.* Geochem. Geophys. Geosyst., 22, e2021GC009812, doi: 10.1029/2021GC009812.

Johnson K., Pagani M. and Ettore A.; 2021: *Probabilistic seismic hazard analysis (PSHA) training manual.* GEM Foundation, doi: 10.13117/OQ_HAZARD_TRAINING_MANUAL.

Johnson K., Villani M., Bayliss K., Brooks C., Chandrasekhar S., Chartier T., Chen Y., Garcia-Pelaez J., Gee R., Styron R., Rood A., Simionato M. and Pagani M.; 2023: *Global Earthquake Model (GEM) seismic hazard map (version 2023.1 - June 2023)*. Doi: 10.5281/zenodo.8409647.

Jost B.M., Webb M. and White L.T.; 2018: *The Mesozoic and Palaeozoic granitoids of north-western New Guinea.* Lithos, 312-313, 223-243, doi: 10.1016/j.lithos.2018.04.027.

Kenyo B., Koumetio F., Kwekam M. and Kengni L.; 2023: *Characteristics of lineaments using gravity data in the eastern Cameroon: structural, hydrogeological and natural risks implications.* J. Afr. Earth Sci., 202, 104886, doi: 10.1016/j.jafrearsci.2023.104886.

Lewerissa R., Rumakey R., Syakur Y.A. and Lapono L.; 2021: *Completeness magnitude (Mc) and b-value characteristics as important parameters for future seismic hazard assessment in the West Papua province, Indonesia.* Arabian J. Geosci., 14, 2588, doi: 10.1007/s12517-021-08885-4.

Lewerissa R., Sismanto and Lapono L.A.S.; 2023: *Identification of sediment-basement structure in West Papua province, Indonesia, using gravity and magnetic data inversion as an Earth's crust stress indicator.* Acta Geophys., 71, 209-226, doi: 10.1007/s11600-022-00913-5.

Li J., Li J., Li W., Xu Z. and She A.; 2025: *Lithospheric structure beneath Tibet based on gravity data from World Gravity Map 2012.* J. Asian Earth Sci., 278, 106411, doi: 10.1016/j.jseaes.2024.106411.

Li Y. and Oldenburg D.W.; 1996: *3D inversion of magnetic data.* Geophys., 61, 394-408, doi: 10.1190/1.1443968.

Maden N. and Elmas A.; 2022: *Major tectonic features and geodynamic setting of the Black Sea Basin: evidence from satellite-derived gravity, heat flow, and seismological data.* Tectonophys., 824, 229207, doi: 10.1016/j.tecto.2022.229207.

Makrup L., Hariyanto A. and Winarno S.; 2018: *Seismic hazard map for Papua Island.* Int. Rev. Civil Eng. (IRECE), 9, 57, doi: 10.15866/irece.v9i2.14090.

Malagnini L. and Munafò I.; 2018: *On the relationship between ML and Mw in a broad range: an example from the Apennines, Italy.* Bull. Seismol. Soc. Am., 108, 1018-1024, doi: 10.1785/0120170303.

PuSGeN (National Center for Earthquake Studies); 2017: *Peta Sumber dan Bahaya Gempa Indonesia Tahun 2017.* Pusat Litbang Perumahan dan Pemukiman, Badan Penelitian dan Pengembangan, Kementerian PUPR, Bandung, Indonesia, 376 pp. (in Indonesian).

Rahman M.M. and Bai L.; 2018: *Probabilistic seismic hazard assessment of Nepal using multiple seismic source models.* Earth Planet. Phys., 2, 327-341, doi: 10.26464/epp2018030.

Reasenberg P.; 1985: *Second-order moment of central California seismicity, 1969–1982.* J. Geophys. Res., 90, 5479–5495, doi: 10.1029/JB090iB07p05479.

Reyes C. and Wiemer S.; 2019: *ZMAP7, a refreshed software package to analyze seismicity.* In: Proc. EGU General Assembly, EGU2019, Vienna, Austria, Geophys. Res. Abstracts, 21, 13153, <ui.adsabs.harvard.edu/abs/2019EGUGA..2113153R>.

Sabahi M., Mahdi Khatib M. and Djamour Y.; 2024: *Spatial and temporal changes of b-value, fractal analysis and stress tensor inversion in the Sistan and Makran zones, eastern and southeastern Iran.* J. Asian Earth Sci., 264, 106038, doi: 10.1016/j.jseaes.2024.106038.

Safani J., Ibrahim K., Deni W., Rubaiyn A., Firdaus F. and Harisma H.; 2023: *Interpreting structural configuration of the Sengkang Basin of Indonesia using edge detection and 3D Euler deconvolution to satellite gravity data.* Turk. J. Earth Sci., 32, 894-914, doi: 10.55730/1300-0985.1881.

Schorlemmer D., Wiemer S. and Wyss M.; 2005: *Variations in earthquake-size distribution across different stress regimes.* Nature, 437, 539-542, doi: 10.1038/nature04094.

Scordilis E.M.; 2006: *Empirical global relations converting Ms and mb to moment magnitude.* J. Seismol., 10, 225-236, doi: 10.1007/s10950-006-9012-4.

Sokolov V., Zahran H.M. and Toni M.; 2024: *Areal-source and fault-source based probabilistic seismic hazard analysis using characteristic earthquake model and Monte-Carlo approach: an example of the Gulf of Aqaba region.* Soil Dyn. Earthquake Eng., 186, 108941, doi: 10.1016/j.soildyn.2024.108941.

Spector A. and Grant F.S.; 1970: *Statistical models for interpreting aeromagnetic data.* Geophys., 35, 293-302, doi: 10.1190/1.1440092.

Thanh Pham L., Anh Nguyen D., Eldosouky A.M., Abdelrahman K., Van Vu T., Al-Otaibi N., Ibrahim E. and Kharbish S.; 2021: *Subsurface structural mapping from high-resolution gravity data using advanced processing methods.* J. King Saud Univ. Sci., 33, 101488, doi: 10.1016/j.jksus.2021.101488.

Watkinson I.M. and Hall R.; 2017: *Fault systems of the eastern Indonesian triple junction: evaluation of Quaternary activity and implications for seismic hazards.* Geol. Soc. London, Spec. Publ., 441, 71–120, doi: 10.1144/SP441.8.

Webb M., White L.T., Jost B.M., Tiranda H. and BouDagher-Fadel M.; 2020: *The history of Cenozoic magmatism and collision in NW New Guine*a - N*ew insights into the tectonic evolution of the northernmost margin of the Australian Plate.* Gondwana Res., 82, 12-38, doi: 10.1016/j.gr.2019.12.010.

White L.T., Morse M.P. and Lister G.S.; 2014: *Lithospheric-scale structures in New Guinea and their control on the location of gold and copper deposits.* Solid Earth, 5, 163-179, doi: 10.5194/se-5-163-2014.

Wiemer S. and Wyss M.; 2000: *Minimum magnitude of completeness in earthquake catalogs: examples from Alaska, the Western United States, and Japan*. Bull. Seismol. Soc. Am., 90, 859–869, doi: 10.1785/0119990114.

Zhao S., McClusky S., Cummins P.R., Miller M.S. and Nugroho H.; 2023: *New insights into crustal deformation of the Indonesia-Australia-New Guinea collision zone from a broad-scale kinematic model.* J. Geophys. Res.: Solid Earth, 128, e2022JB024810, doi: 10.1029/2022JB024810.

Corresponding author: Richard Lewerissa
Department of Physics, Faculty of Mathematics and Natural Sciences, Papua University
Manokwari, Papua Barat 98314, Indonesia
Phone: +821 367 43033; e-mail: r.lewerissa@unipa.ac.id